DEVELOPMENT OF A THEORY OF THE SPECTRAL REFLECTANCE OF MINERALS
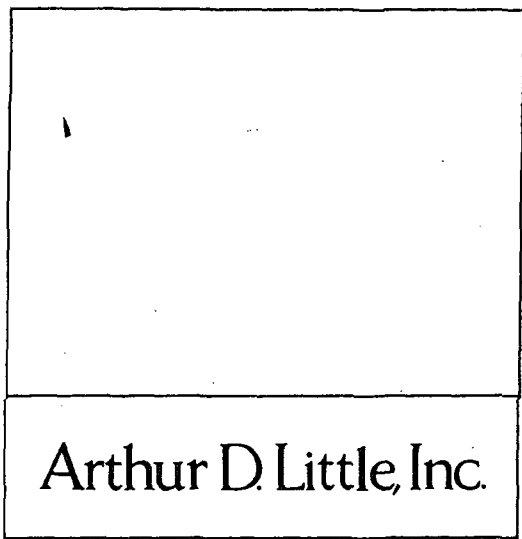
PART IV

FINAL REPORT

by

J. R. ARONSON, A. G. EMSLIE, E. M. SMITH

OCTOBER 1972

NAS 9-10875

ADL C-72594

Arthur D. Little, Inc.

DEVELOPMENT OF A THEORY

OF THE SPECTRAL REFLECTANCE OF MINERALS

PART IV

FINAL REPORT

By

J. R. Aronson, A. G. Emslie, and E. M. Smith

Prepared for

National Aeronautics and Space Administration
Manned Spacecraft Center
Houston, Texas   77058

Contract NAS 9-10875

ADL C-72594

October 1972

Arthur D. Little, Inc.

Abstract

This report describes the results of a research program directed toward the development of a theory of the spectral reflectance or emittance of particulate minerals. The theory is expected to prove invaluable in the detailed interpretation of the remote infrared spectra of planetary surfaces. The principal results are described in two manuscripts that have been submitted for publication (Sections II and III). Some further improvements and other results are discussed in other sections.

Table of Contents

List of Figures

I. INTRODUCTION

The results of our research program directed at the development of a theory of the spectral reflectance of minerals have been discussed in a series of reports[1,2,3] as the work has proceeded. These progress reports have continually updated the theory as successive refinements were made. During the course of the work certain lines of investigation were pursued while others were abandoned without perhaps being sufficiently explored. Frequently, improvements in the fit to certain spectral features were made at the expense of other details, but as the improvements were almost always in the nature of a less approximate treatment, and as the apparent fit showed distinct overall improvements, the authors believe that the theory has continually improved. A thorough description of the details of the work, as of the summer of 1972, has been submitted for publication in Applied Optics. This description takes the form of two papers. The first provides a coherent description of the entire theory and the second shows the results of comparison of that theory with experimental data. For the most part these are up-to-date and are therefore herein presented as the bulk of the final report on this work. Nonetheless in the few months remaining after their submission some further improvements were made in the theory. They will be discussed along with some topics not treated in the papers. It is the authors' intention to write a further paper to discuss these topics and improvements when they have sufficiently matured.

References

1. J. R. Aronson and A. G. Emslie, "Development of a Theory of the Spectral Reflectance of Minerals," Report to NASA, Manned Spacecraft Center, October 1969 (Contract NAS 9-8396).

2. J. R. Aronson, A. G. Emslie, L. H. Roach, P. F. Strong, and P. C. von Thüna, "Development of a Theory of the Spectral Reflectance of Minerals, Part II," Report to NASA, Manned Spacecraft Center, April 1971 (Contract NAS 9-10875).

3. J. R. Aronson, A. G. Emslie, L. H. Roach, E. M. Smith and P. C. von Thüna, "Development of a Theory of the Spectral Reflectance of Minerals, Part III," Report to NASA, Manned Spacecraft Center, January 1972 (Contract NAS 9-10875).

II. The Spectral Reflectance and Emittance
of Particulate Materials,

Part I - Theory

A. G. Emslie and J. R. Aronson

Arthur D. Little, Inc.

Cambridge, Massachusetts   02140

Abstract

The infrared spectral reflectance of a semi-infinite medium
composed of irregular particles of different materials is cal-
culated in terms of the sizes, shapes, and complex refractive in-
dices of the particles. For particles larger than the wavelength
the scattering and absorption are computed mainly by geometrical
optics but with important wave-optical corrections for the addi-
tional absorption caused by edges and asperities, which are repre-
sented by dipoles distributed over the surface of the particle.

For particles smaller than the wavelength a Lorentz-Lorenz model
is used to derive the average complex index of the medium, the
particles being treated as ellipsoids with a wide range of shapes.
The average scattering of an individual ellipsoidal particle is
then found from the relative refractive index of the particle
with respect to the Lorentz-Lorenz medium. For both large and
small particles the single-particle scattering is represented by
six discrete beams. Calculation of the reflectance is then
facilitated by a radiative transfer method that also involves six
beams. For particles of intermediate size a suitable formula
bridging the results for large and small particles is found to
be satisfactory.

INTRODUCTION

Many theoretical attempts have been made to explain the reflection spectra of clouds and powders.[1,2] Most authors calculate the scattering and absorption of the individual particles by applying the well-known Mie[3] theory to spheres of the same volume as the actual particles.[4] The reflectance of the cloud or powder is then calculated by a two-beam theory such as that of Schuster[5] or Kubelka and Munk,[6] by a many-beam method usually based on the general theory of Chandrasekhar,[7] or by a Monte Carlo technique.[8] Blevin and Brown[9] have demonstrated that multiple-beam calculations, in which scattering and absorption are regarded as spatially continuous, remain approximately valid even when the particles are almost in contact. Non-continuum models have, however, been proposed by Lathrop[10] and Melamed.[11]

This paper presents a theory of spectral reflectance in which two additional physical mechanisms are taken into account, namely, the effect of particle shape and, in the case of closely-spaced

fine particles, the effect of coherent interaction between the particles. Inclusion of these two effects is essential to provide good agreement between theoretical and experimental spectra, as shown in Part II.[12] In addition, the theory incorporates a number of mathematical innovations.

In order to allow for shape features such as edges and surface asperities on large particles $(d \geq \lambda)$ we abandon Mie theory and revert to a combination of geometrical optics to obtain the main scattering and absorption, and wave optics to obtain the effect of the edges and asperities, both regarded as induced dipoles. This we will refer to as the coarse particle theory.

In the case of fine closely-spaced particles $(d \ll \lambda)$, we also do not use Mie theory but regard the particles as randomly oriented ellipsoidal dipoles which cause both coherent scattering (Fresnel component) and incoherent scattering (Rayleigh component). This we call the fine particle theory. The coarse and fine theories are connected by an empirical bridging formula.

Arthur D Little, Inc

COARSE PARTICLE THEORY

As a model for the coarse particle theory we represent the large-scale shape of a particle by a sphere of the same volume as the actual particle and the small-scale shape, including edges and other surface asperities, as a distribution of dipoles spread uniformly over the surface of the sphere. This model evolved from the practical requirement of mathematical tractability and from the consideration that, for chunky particles at least, the scattering and absorption corsssections depend critically on the small-scale shape but only slightly on the large-scale shape. Final justification of the model appears in the good agreement between theory and experiment. One might think that an equivalent sphere would be a poor representation of a platelet-shaped particle but even in this extreme case the theory gives results in good agreement with observation.

1. Calculation of Single-Particle Scattering and Absorption

Crosssections

We first consider a parallel beam of radiation incident on the equivalent sphere which represents a given particle. Fig. 1 shows reflected and refracted rays produced by an incident ray that strikes the sphere at an angle of incidence θ.

In order to allow for the effect of inhomogeneous wave propagation that occurs owing to the complex index of refraction

$$m = n - ik \qquad (1)$$

we define the effective angle of refraction ψ as the direction of the Poynting vector in the particle, given by the formula

$$\tan \psi = \frac{\sin \theta}{\text{Re } (m^2 - \sin^2\theta)^{1/2}} \qquad (2)$$

where Re signifies "real part". Eq. (2) reduces to the usual law of refraction when m is real, i.e., when the absorption index k is zero.

The angle of deviation ϕ of the transmitted ray is given by the relation

$$\phi = 2 \, | \, \theta - \psi \, | \qquad (3)$$

Arthur D Little, Inc.
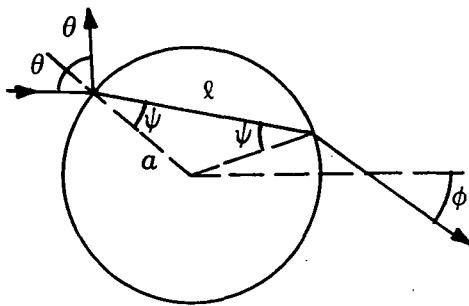
FIGURE 1   RAY TRACING GEOMETRY

where the absolute value signs allow for the case where $n < 1$.

The transmission path ℓ is given by the equation

$$\ell = 2a \cos\psi \qquad (4)$$

where a is the radius of the sphere.

Let I_o be the intensity of the unpolarized incident parallel

beam. Then the power incident on the sphere in the angular range

$d\theta$ is

$$dP_o = \pi a^2 I_o \sin 2\theta \, d\theta \qquad (5)$$

The corresponding refracted power is

$$(dP)_{refr} = \pi a^2 I_o T_o^2 T \sin 2\theta \, d\theta \qquad (6)$$

where T_o is the surface transmittance which includes the effects of

Fresnel reflection and absorption by asperities and edges, and T is

the transmission factor given by

$$T = e^{-\frac{4\pi k \ell}{\lambda}} \qquad (7)$$

where λ is the free-space wavelength of the radiation. An expres-

sion for T_o is derived later.

Arthur D Little, Inc.

The angular distribution (6), considered as function of the angle of deviation ϕ given by (3), is the contribution of refraction to the single particle phase function. To facilitate radiative transfer calculations we represent the continuous distribution (6) approximately by a set of six mutually perpendicular discrete beams comprising a forward-scattered beams, a backward-scattered beam and four transversely-scattered beams. For this purpose we need a method for dividing the power dP of a ray in the forward hemisphere between the forward and transverse discrete beams. Suitable weighting factors are $\cos^2\phi$ for the forward direction and $\sin^2\phi$ for the combined transverse directions since this division clearly conserves energy and is exact for $\phi = 0$, $45°$, and $90°$. For a ray in the backwards ($\phi \geq 90°$) hemisphere the backwards and transverse weighting factors are also $\cos^2\phi$ and $\sin^2\phi$. In the case of isotropic scattering the weighting scheme results in equal intensities in the six discrete beams as it should.

Using this weighting method we find from (6) that the cross-

sections for forward, transverse, and backward scattering due to

refraction are

$$\sigma_{\text{refr, f}} = \pi a^2 \int\limits_{\phi \le \pi/2} T_o^2 T \cos^2\phi \sin 2\theta \, d\theta \tag{8}$$

$$\sigma_{\text{refr, t}} = \pi a^2 \int\limits_{\theta=0}^{\pi/2} T_o^2 T \sin^2\phi \sin 2\theta \, d\theta \tag{9}$$

$$\sigma_{\text{refr, b}} = \pi a^2 \int\limits_{\phi \ge \pi/2} T_o^2 T \cos^2\phi \sin 2\theta \, d\theta \tag{10}$$

The crosssections for externally reflected radiation are

given similarly by

$$\sigma_{\text{refl, f}} = \pi a^2 \int\limits_{\pi/4}^{\pi/2} R_o \cos^2 2\theta \sin 2\theta \, d\theta \tag{11}$$

$$\sigma_{\text{refl, t}} = \pi a^2 \int\limits_{o}^{\pi/2} R_o \sin^2 2\theta \sin 2\theta \, d\theta \tag{12}$$

$$\sigma_{\text{refl, b}} = \pi a^2 \int\limits_{o}^{\pi/4} R_o \cos^2 2\theta \sin 2\theta \, d\theta \tag{13}$$

where R_o, the surface reflectance, like T_o, includes the effects

of both Fresnel reflection and absorption by asperities and edges,

and will be calculated later. These two quantities, as well as T,

vary with wavelength since they depend on m which is a function

of the wavelength. The weighting factors $\cos^2\phi$ and $\sin^2\phi$ in this

case become $\cos^2 2\theta$ and $\sin^2 2\theta$ since $\phi = \pi - 2\theta$ for reflection.

A third contribution to the crosssections arises from radia-

tion that undergoes one or more internal reflections in the par-

ticle. For a given incident ray the fraction of the power that

emerges from the particle after undergoing internal reflections

is the sum of the series $R_o T_o^2 T^2 + R_o^2 T_o^2 T^3 + \ldots\ldots$ which has

the value $R_o T_o^2/(1-R_o T)$. We assume for simplicity that this power

is distributed isotropically so that the weighting factors are the

same for all six discrete beams. The crosssections for iternally

reflected radiation are therefore

$$\sigma_{\text{int refl, f}} = \frac{1}{6}\,\pi a^2 \int_o^{\pi/2} \frac{R_o T_o^2 T^2}{1-R_o T}\ \sin 2\theta\ d\theta \qquad (14)$$

$$\sigma_{\text{int refl, t}} = \frac{4}{6}\,\pi a^2 \int_o^{\pi/2} \frac{R_o T_o^2 T^2}{1-R_o T}\ \sin 2\theta\ d\theta \qquad (15)$$

Arthur D Little, Inc.

$$\sigma_{int\ refl,\ b} = \frac{1}{6}\ \pi a^2 \int_0^{\pi/2} \frac{R_o T_o^2 T^2}{1-R_o T}\ \sin 2\theta\ d\theta \tag{16}$$

To calculate the absorption crosssection we subtract the sum

of the factors $T_o^2 T$, R_o, and $R_o T_o^2 T^2/(1-R_o T)$ from unity and inte-

grate over θ. Therefore

$$\sigma_{abs} = \pi a^2 \int_0^{\pi/2} (1 - R_o - \frac{T_o^2 T}{1-R_o T})\ \sin 2\theta\ d\theta \tag{17}$$

Some comments are in order on how our procedure compares with

current methods. The scheme of applying weighting factors directly

to the phase function in order to derive a set of discrete beams

differs from the usual method in which the phase function is first

expanded in a series of Legendre polynomials which is then truncated,

generally after two terms. It is to be noted that the reconsti-

tuted phase function obtained from the truncated series may differ

very considerably from the original phase function, especially in

the case of strong forward scattering. For complete forward scat-

tering the truncated phase function is proportional to $1 + 3\ \cos\phi$

which actually yields a negative intensity in the backward direc-

tion ($\phi = \pi$). We believe that our procedure is preferable since it cannot give rise to any such non-physical intensity distribution.

The Mie theory, which is widely applied at present for phase function calculations of both spherical and non-spherical particles, cannot be made to include the important effects of edges and other asperities. The reason is that R_0 and T_0, which contain these effects, occur in different ways in the expressions for the cross-sections for reflection, refraction, internal reflection, and absorption.

In our treatment we omit the effect of diffraction around a particle on the ground that for powders, on which most of our experimental work has been done, the particles are so close together and so randomly distributed that the conditions for Fraunhofer diffraction do not exist. In the case of clouds, however, a correction for diffraction should be made.

2. Effect of Edges and Asperities

The surface reflection and transmission factors R_0 and T_0

Arthur D Little, Inc.

depend on the effect of edges and asperities on the particles as well as on the ordinary Fresnel reflectance. In Part II[12] we show experimentally that very fine particles adhering to the larger particles in a coarse powder cause a substantial reduction in reflection level. Another experiment shows that a similar loss occurs in the reflectance of a single crystal when the surface of the crystal is abraded. Moreover, the spectral reflectance of the abraded crystal has a broad feature that closely resembles a feature in the spectrum of a coarse powder of the same material. Microscopic examination of this powder shows that the particles have, in addition to the expected sharp edges, facets that are covered with fine steps, ridges, and other asperities. Another powder composed of spherical particles which have surface asperities but no edges has a smaller reflection loss than a powder of jagged particles. These facts prove that any perturbation of the smooth surface of a particle, whether in the form of an edge, an asperity, or an adhering smaller particle, causes enhanced absorption.

Arthur D Little, Inc

We have considered several possible mechanisms for the enhanced absorption. One idea is that asperities and edges act like a transition layer with a graded refractive index that provides a partial impedance match between vacuum and the interior of the particles. Another concept is that in spectral regions of near-total external reflection, which occurs when $n < 1$, the inhomogeneous wave traveling tangentially just under the surface of the particle is scattered by asperities and edges into the interior of the particles, where it is absorbed. A third possibility is that the asperities and edges act as induced dipoles and absorb some of the incident radiation directly.

In view of the fact that the phenomenon of excessive absorption is observed when the asperities or adhering particles are much smaller than the wavelength we conclude that direct dipole absorption is the most likely mechanism. The reason is that under these conditions dipole absorption is directly proportional to the volume of an asperity while scattering varies as the square of the

Arthur D Little, Inc.

volume. Impedance matching requires a transition layer whose thickness is an appreciable fraction of a wavelength. In this paper, we will therefore confine our calculations to the case of direct absorption by surface dipoles. This subject has been investigated in some depth by Strachan[13] and Berreman.[14] We find, however, that a simpler theory, in which we ignore interactions of the dipoles with each other and with the underlying main particle, serves our purposes very well.

We assume that edges and asperities can be represented as ellipsoidal particles. An ellipsoidal sub-particle of electric susceptibility χ placed in an electric field E acquires a polarization P given by the well-known result of electrostatics:

$$P_x = \frac{\chi}{1+L\chi} \ E_x \tag{18}$$

$$P_y = \frac{\chi}{1+M\chi} \ E_y \tag{19}$$

$$P_z = \frac{\chi}{1+N\chi} \ E_z \tag{20}$$

where the components P_x, P_y, P_z and E_x, E_y, E_z of P and E are re-

ferred to coordinates aligned with the principal axes of the ellip-

soid. The depolarization factors L, M, N are determined by the

axial ratios of the ellipsoid and satisfy the relation

$$L + M + N = 4\pi \tag{21}$$

In the case of a sphere $L = M = N = 4\pi/3$.

From (18)-(20) one finds for the components of the induced

dipole moment μ:

$$\mu_x = \frac{V(K-1)E_x}{4\pi + L(K-1)} \tag{22}$$

$$\mu_y = \frac{V(K-1)E_y}{4\pi + M(K-1)} \tag{23}$$

$$\mu_z = \frac{V(K-1)E_z}{4\pi + N(K-1)} \tag{24}$$

where V is the volume of the particle and K is its dielectric con-

stant.

We assume that the particle is small enough so that (22)-(24)

remain approximately valid for an alternating field. Then the

power absorbed by the particle is

$$W = \frac{1}{2} \, \mathrm{Re}\,(E \cdot \frac{d\mu}{dt})$$

$$= - \frac{\omega}{2} \, \mathrm{Im}(E_x \mu_x + E_y \mu_y + E_z \mu_z)$$

$$= - \frac{\omega}{2} \, \mathrm{Im} \left\{ \frac{(K-1)|E_x|^2}{4\pi + L(K-1)} + \frac{(K-1)|E_y|^2}{4\pi + M(K-1)} + \frac{(K-1)|E_z|^2}{4\pi + N(K-1)} \right\} \qquad (25)$$

We next assume that the particle can have all orientations

relative to the field E. Then the average power absorbed is

$$\overline{W} = - \frac{\omega V |E|^2}{6} \, \mathrm{Im}(m^2 - 1) \left\{ \frac{1}{4\pi + L(m^2-1)} + \frac{1}{4\pi + M(m^2-1)} + \frac{1}{4\pi + N(m^2-1)} \right\} \qquad (26)$$

where ω is the angular frequency of the radiation and we have re-

placed K by the square of the complex refractive index, m.

It is to be noted that for a given shape of ellipsoid, speci-

fied by particular values of L, M, and N, $\overline{W}$ becomes very large at

wavelengths for which m is near the poles of the expression in

curly brackets in (26), i.e., when $n \ll 1$ and k is near $[(4\pi/L)-1]^{1/2}$,

$[(4\pi/M)-1]^{1/2}$, or $[(4\pi/N)-1]^{1/2}$. Such values of m actually occur

in strong reststrahlen spectral regions in the infrared. There-

fore reflection spectra calculated for edges or asperities repre-

Arthur D Little, Inc.

sented by a particular choice of L, M, and N show very sharp de-

creases in reflectance at wavelengths for which m is close to these

special values of m, while experimental spectra show much broader

absorption maxima in the same regions of the spectrum. It is

clear therefore that in the theory one must allow for the observed

variability in the shapes of edges and asperities by averaging

over a range of values L, M, and N. We have tried averaging Eq.

(26) over various ranges of L, M, and N subject, of course, to

condition (21). The result is that the widths of the absorption

maxima now become similar to those observed experimentally, pro-

vided that the range of integration over L, M, and N is wide enough.

Apart from this requirement one still has considerable freedom in

the choice in the range of ellipsoid shapes included in the average,

as determined by L, M, and N values covered. Different ellipsoid

shape distributions produce subtle differences in the shape of

the theoretical reflectance spectrum.

In the case of edges we choose ellipsoids that are very elon-
gated in the direction of the edge, corresponding to $N = 0$, and
with a complete range of cross-sectional shapes. Under these con-
ditions, $M = 4\pi - L$ and L varies from 0 to 4π. On averaging (26)
over all values of L with equal weighting we obtain for the power
absorbed by an edge:

$$\overline{\overline{W}}_e = - \frac{\omega V_e |E|^2}{24\pi} \text{ Im } (m^2 - 1 + 4 \log m) \tag{27}$$

In the case of surface asperities where the shapes may vary
from ridges to mounds we select ellipsoids of revolution ($L = M$)
and let N vary from 0 (needle shape) to $4\pi/3$ (sphere). The aver-
age value of $\overline{W}$ for asperities is then

$$\overline{\overline{W}}_a = - \frac{\omega V_a |E|^2}{24\pi} \text{ Im } (12 \log \frac{m^2+1}{2} - 9 \log \frac{m^2+2}{3}) \tag{28}$$

We must next consider the value to be assigned to the volume
V of asperities or edges. In the case of asperities we could take
V_a to be twice the actual volume of a ridge or bump on the sur-

face in order to allow approximately for the image field. In practice, however, since the details of the size distribution of the asperities are difficult to obtain we regard V as an adjustable constant.

In the case of edges V can be expressed as

$$V_e = \ell_e \; \delta \; b \tag{29}$$

where ℓ_e, δ, and b are respectively the edge length, the effective depth of penetration of the radiation, and the effective width of the region perturbed by the presence of the edge.

We assume that both δ and b are of the order of $\lambda/4\pi$, where λ is the free-space wavelength of the radiation, except that in spectral regions of high absorption δ should become considerably smaller than b owing to reduced penetration of the radiation. This behaviour in absorbing regions is obtained if we equate δ to the $1/e$ penetration depth of the Poynting vector associated with the refracted wave, which, for an average angle of incidence of 45°, is

given by

$$\delta = \frac{\lambda}{4\pi \, Re \, (0.5 - m^2)^{1/2}} \tag{30}$$

However, since this expression diverges when the medium is transparent and $n > 1/\sqrt{2}$, we replace (30) by the modified expression

$$\delta = \frac{\lambda}{4\pi} \left(1 - e^{-\frac{1}{Re \, (0.5 - m^2)^{1/2}}} \right) \tag{31}$$

which reduces to (30) in highly absorbing regions and is approximately $\lambda/4\pi$ in transparent regions.

We now calculate the surface absorptance of a particle. The power density I_o of the incident parallel beam is given by

$$I_o = \frac{c |E|^2}{8\pi} = \frac{\omega \lambda |E|^2}{16\pi^2} \tag{32}$$

The average surface absorptance caused by edges and asperities for locations on the equivalent spherical particle corresponding to the angle of incidence θ is given by the expression

$$A_o = 1 - e^{-X} \tag{33}$$

where

$$X = \frac{N_e \, \overline{\overline{W}}_e + N_a \, \overline{\overline{W}}_a}{I_o \, \cos\theta} \tag{34}$$

Arthur D Little, Inc

Here N_e and N_a are the average number of edges and asperities per unit area of the spherical surface. The obliquity factor $1/\cos\theta$ allows for the increase in the number of edges and asperities per unit crosssection of the beam as θ increases. The exponential form of (33) ensures that A_o always lies between 0 and 1 and has the correct value when $\overline{\overline{W}}_e$ and $\overline{\overline{W}}_a$ are small.

The surface reflectance and transmittance are related to A_o by the equations

$$R_o = \left(\frac{R_s + R_p}{2}\right)(1 - A_o) \tag{35}$$

$$T_o = \left(1 - \frac{R_s + R_p}{2}\right)(1 - A_o) \tag{36}$$

where R_s and R_p are the Fresnel reflectances at the angle of incidence θ for the two states of polarization of the incident radiation. It will be noticed that (35) and (36) reduce to the usual expressions in the absence of edges or asperities. The equations also satisfy energy conservation since

$$R_o + T_o + A_o = 1 \tag{37}$$

From (27), (28), (29) and (32), Equation (34) becomes

$$X = \frac{2\pi}{3\lambda \cos\theta} \left\{ -N_e \ell_e \delta b \; Im(m^2 - 1 + 4 \log m) \right.$$
$$\left. - N_a V_a Im(12 \log \frac{m^2 + 1}{2} - 9 \log \frac{m^2 + 2}{3}) \right\} \quad (38)$$

In this expression we consider $N_a V_a$, the total volume of asperities

per unit area of particle surface, as an adjustable parameter.

Likewise b, the effective width of an edge, is adjustable to some

extent from a nominal value of $\lambda/4\pi$.

The product $N_e \ell_e$, which is the total length of all the edges

of a particle divided by the surface area of the equivalent sphere,

depends on the geometry of the particle. Values of this quantity,

expressed in terms of the diameter d of the equivalent sphere, are

shown in Table I for the five regular polyhedra. It is to be noted

that for any given particle shape the edge absorption depends in-

versely on d. As one would expect, the proportionality constant

increases, albeit erratically, as the number of edges increases.

Since the dodecahedron and icosahedron have unlikely geometries

we take $N_e \ell_e$ to be the mean for the first three polyhedra:

$$N_e \ell_e = \frac{3.4}{d} \tag{39}$$

Table I. Total Edge Length per Unit Area of Equivalent Sphere

Particle Shape	Number of Edges	$N_e \ell_e$
Tetrahedron	6	3.14/d
Cube	12	3.08/d
Octahedron	12	3.96/d
Dodecahedron	30	3.90/d
Icosahedron	30	5.93/d

FINE PARTICLE THEORY

Closely spaced fine particles of size much smaller than a wavelength interact in two ways with a beam of radiation. First, many particles scatter coherently in the beam direction and thereby give rise to an average Lorentz-Lorenz (L.L.) index of refrac-

Arthur D Little, Inc.

tion for the particulate medium, which causes Fresnel reflection

at the surface of the medium. Second, since the particles are

not regularly spaced as in a crystal each particle also scatters

the radiation incoherently in all directions (Rayleigh Scattering)

with an intensity that depends on the contrast between the in-

trinsic refractive index of a given particle and the L.L. index of

the averaged medium in which it is embedded. The fine particle

theory includes both of these effects.

1. The Lorentz-Lorenz Index of Refraction

Our model for a fine-particle powder consists of an assembly

of ellipsoids of the same volume as the actual particles and cover-

ing a wide range of shapes. The reasons for this choice of model

are that ellipsoids are mathematically tractable by the L.L. method

and that an average over a range of ellipsoid shapes avoids "reso-

nance" difficulties of the kind already mentioned in connection

with edge and asperity dipoles. Such difficulties previously led

us[15, 16, 17] to calculate excessively high Fresnel reflectances

when the L.L. method was used for spherical shapes alone.

By analogy with the original L.L. method we consider a particular ellipsoid to be enclosed in a coaxial ellipsoidal cavity of the same shape carved out of a continuous medium that has the average L.L. index $\bar{m}$. If $\bar{E}$ is the average electric field in the medium then the field E_c in the cavity has the components

$$E_x^c = \bar{E}_x(1 + L\bar{\chi}) \tag{40}$$

$$E_y^c = \bar{E}_y(1 + M\bar{\chi}) \tag{41}$$

$$E_z^c = \bar{E}_z(1 + N\bar{\chi}) \tag{42}$$

where $\bar{\chi}$ is the electric susceptibility of the medium and L, M, and N are the depolarization factors of the cavity and of the ellipsoid. The axes (x, y, z) are aligned with the axes of the ellipsoid.

The field E^c in the cavity produces a polarization P in the particle with components

$$P_x = \frac{\chi E_x^c}{1 + L\chi} = \frac{\chi(1 + L\bar{\chi})\bar{E}_x}{1 + L\chi} \tag{43}$$

$$P_y = \frac{\chi E_y^c}{1 + M\chi} = \frac{\chi(1 + M\bar{\chi})\bar{E}_y}{1 + M\chi} \tag{44}$$

$$P_z = \frac{XE_z^c}{1 + NX} = \frac{X(1 + N\overline{X})\overline{E}_z}{1 + NX} \qquad (45)$$

We now assume that the ellipsoid has random orientation with respect to the field $\overline{E}$ in the medium and calculate the average polarization of the ellipsoid in the direction of $\overline{E}$. The result is

$$\overline{P} = \frac{<P \cdot \overline{E}>}{|\overline{E}|} = \frac{X|\overline{E}|}{3}\left(\frac{1 + L\overline{X}}{1 + LX} + \frac{1 + M\overline{X}}{1 + MX} + \frac{1 + N\overline{X}}{1 + NX}\right) \qquad (46)$$

The average electric moment induced in the ellipsoid is therefore

$$\overline{\mu} = \frac{X|\overline{E}|V}{3}\left(\frac{1 + L\overline{X}}{1 + LX} + \frac{1 + M\overline{X}}{1 + MX} + \frac{1 + N\overline{X}}{1 + NX}\right) \qquad (47)$$

where V is the volume of the ellipsoid.

Next we average $\overline{\mu}$ with respect to ellipsoid shape. For this purpose we assume that all values of L, M, and N from 0 to 4π are equally probable subject to the constraint that $L + M + N = 4\pi$.

The result of the averaging is

$$\overline{\overline{\mu}} = |\overline{E}|V\left\{\overline{X} + \frac{1}{2\pi}\left(1 - \frac{\overline{X}}{X}\right)\left[\left(1 + \frac{1}{4\pi X}\right)\log\left(1 + 4\pi X\right) - 1\right]\right\} \qquad (48)$$

We can also write the relation

$$\overline{X} = \frac{f\overline{\overline{\mu}}}{V|\overline{E}|} \qquad (49)$$

Arthur D Little, Inc.

since the whole medium can be considered to be composed of ellipsoids of average dipole moment $\bar{\bar{\mu}}$ packed at the volume fraction f.

On substituting for $\bar{\bar{\mu}}$ from (48) into (49) and solving for $\bar{\chi}$ we obtain the result

$$2\pi\bar{\chi} = \frac{f\left[(1 + \frac{1}{4\pi\chi}) \log (1 + 4\pi\chi) -1\right]}{1 - f + \frac{f}{2\pi\chi}\left[(1 + \frac{1}{4\pi\chi}) \log (1 + 4\pi\chi) -1\right]} \tag{50}$$

Since $4\pi\bar{\chi} = \bar{m}^2 - 1$ and $4\pi\chi = m^2 - 1$ we obtain the following relation between the L.L. index $\bar{m}$ and the particle index m:

$$\bar{m}^2 = 1 + \frac{2f\left[(1 + \frac{1}{m^2-1}) \log (m^2) - 1\right]}{1 - f + \frac{2f}{m^2-1}\left[(1 + \frac{1}{m^2-1}) \log(m^2) - 1\right]} \tag{51}$$

It is worth noting that $\bar{m} \rightarrow m$, as it should, when $f \rightarrow 1$.

This formula can readily be generalized for the case of a mixture of fine particles of different materials with volume fractions f_j and indices m_j. The result is

$$\bar{m}^2 = 1 + \frac{2\sum_j f_j\left[(1 + \frac{1}{m_j^2-1}) \log (m_j^2) - 1\right]}{1 - \sum_j f_j + \sum_j \frac{2f_j}{m_j^2-1}\left[(1 + \frac{1}{m_j^2-1}) \log (m_j^2) - 1\right]} \tag{52}$$

2. Rayleigh Scattering Crosssection

The Raleigh scattering by an ellipsoidal particle of index m immersed in a medium of L.L. index $\bar{m}$ depends on the polarizibility of the ellipsoid, which is related to the relative index $m/\bar{m}$ by the formula

$$\alpha_x = \frac{V(\frac{m^2}{\bar{m}^2} - 1)}{4\pi + L(\frac{m^2}{\bar{m}^2} - 1)} \tag{53}$$

with similar expressions for the polarizibilities α_y and α_z along the two other principal axes of the ellipsoid.

The total scattering crosssection for an incident parallel beam of radiation in the medium is given by[18]

$$\sigma = \frac{8\pi}{3} \kappa^4 (\ell^2 |\alpha_x|^2 + m^2 |\alpha_y|^2 + n^2 |\alpha_z|^2) \tag{54}$$

where ℓ, m, n are the direction cosines of the electric field in the medium and

$$\kappa = \frac{2\pi}{\lambda_{medium}} = \frac{2\pi \bar{n}}{\lambda} \tag{55}$$

Here $\bar{n}$ is the real part of the L.L. index $\bar{m}$.

On averaging over all orientations of the ellipsoid relative

Arthur D Little, Inc.

to the electric field direction we find, from (53) and (54):

$$\sigma = \frac{8\pi}{9} \kappa^4 V^2 \left| \frac{m^2}{\bar{m}^2} - 1 \right|^2 \left\{ \left| \frac{1}{4\pi + L\left(\frac{m^2}{\bar{m}^2} - 1\right)} \right|^2 + \left| \frac{1}{4\pi + M\left(\frac{m^2}{\bar{m}^2} - 1\right)} \right|^2 \right.$$

$$\left. + \left| \frac{1}{4\pi + N\left(\frac{m^2}{\bar{m}^2} - 1\right)} \right|^2 \right\} \tag{56}$$

We next average over all ellipsoid shapes as in the derivation of the L.L. index. Under these conditions the three terms containing L, M, and N are equal and (56) reduces to

$$\sigma = \frac{8\pi}{3} \kappa^4 V^2 \left| \frac{m^2}{\bar{m}^2} - 1 \right|^2 \left\langle \left| \frac{1}{4\pi + L\left(\frac{m^2}{\bar{m}^2} - 1\right)} \right|^2 \right\rangle \tag{57}$$

where < > indicates averaging over L.

On carrying out the averaging for $0 \lessgtr L \lessgtr 4\pi$, and allowing for the fact that m and $\bar{m}$ are complex numbers, we obtain

$$\sigma = \frac{\kappa^4 V^2 \left| \frac{m^2}{\bar{m}^2} - 1 \right|^2}{3\pi} \left\{ \frac{\text{Im}\left(\log \frac{m^2}{\bar{m}^2}\right) + \text{Im}\left(\frac{\log \frac{m^2}{\bar{m}^2}}{\frac{m^2}{\bar{m}^2} - 1}\right)}{\text{Im}\left(\frac{m^2}{\bar{m}^2}\right)} \right\} \tag{58}$$

where Im signifies "imaginary part".

One can generalize this expression to include the case of a

mixture of mineral powders (or of particles of the same material

but of different sizes) by multiplying (58) by the particle volume

fraction f_j of material j and summing over j.

RADIATIVE TRANSFER THEORY

The radiative transfer theory presented in this paper is re-

stricted to the calculation of the reflectance of a parallel beam

incident normally on the surface of a semi-infinite powder or cloud.

This case is equivalent, by Kirchhoff's law, to the calculation

of the normal emittance of an isothermal powder or cloud, which

is approximately the measured quantity discussed in Part II.

(1) Six-beam Model

Multiple scattering of the incident parallel beam produces

diffuse radiation in the particulate medium. We represent the

combination of diffuse and collimated radiation at any point in

the medium by means of six mutually orthogonal beams, one of which

Arthur D Little, Inc.

is in the direction of the collimated incident beam which we take to be the x-direction.

Let I and J be the flux densities of the beams in the x and -x directions and I_1, I_2, I_3, I_4 the fluxes in the transverse directions y, -y, z, -z.   Then the radiative transfer equations are

$$\frac{dI}{dx} = -(K + S_b + S_t)I + S_b J + \frac{1}{4} S_t(I_1 + I_2 + I_3 + I_4) \qquad (59)$$

$$-\frac{dJ}{dx} = -(K + S_b + S_t)J + S_b I + \frac{1}{4} S_t(I_1 + I_2 + I_3 + I_4) \qquad (60)$$

$$\frac{dI_1}{dy} = -(K + S_b + S_t)I_1 + S_b I_2 + \frac{1}{4} S_t(I + J + I_3 + I_4) \qquad (61)$$

$$-\frac{dI_2}{dy} = -(K + S_b + S_t)I_2 + S_b I_1 + \frac{1}{4} S_t(I + J + I_3 + I_4) \qquad (62)$$

$$\frac{dI_3}{dz} = -(K + S_b + S_t)I_3 + S_b I_4 + \frac{1}{4} S_t(I + J + I_1 + I_2) \qquad (63)$$

$$-\frac{dI_4}{dz} = -(K + S_b + S_t)I_4 + S_b I_3 + \frac{1}{4} S_t(I + J + I_1 + I_2) \qquad (64)$$

where K, S_b, S_t are the absorption, backscattering, and transverse scattering coefficients, respectively, for any of the beams.

These coefficients will later be expressed in terms of the single-

Arthur D. Little, Inc.

particle crosssections derived above.

Owing to the symmetry of the situation we have:

$$I_1 = I_2 = I_3 = I_4 = \frac{1}{4} P \tag{65}$$

where P is the sum of the transverse fluxes. Therefore, on

adding Equations (61)-(64) we obtain the result

$$P = \frac{S_t}{K + \frac{1}{2} S_t} (I + J) \tag{66}$$

On substituting this value of P into (59) and (60) and re-

arranging the resulting equations we find that they can be put in

the form

$$\frac{dI}{dx} = -(K' + S')I + S'J \tag{67}$$

$$-\frac{dJ}{dx} = -(K' + S')J + S'I \tag{68}$$

where

$$S' = \frac{4KS_b + 2S_bS_t + S_t^2}{4K + 2S_t} \tag{69}$$

$$K' = \frac{4K^2 + 6KS_t}{4K + 2S_t} \tag{70}$$

Thus the radiative transfer problem here reduces essentially

to a two-beam problem with equations which are identical in form

to the well-known equations of Schuster[5] or Kubelka and Munk.[6]

The interpretation of our coefficients K' and S' is different, however, since, from (69) and (70), each involves both absorption and scattering terms which arise from the interaction of the I and J beams with the reservoir of transverse radiation. In the Schuster-Kubelka-Munk equations, on the other hand, K' and S' refer to absorption and backscattering, respectively, of two oppositely-directed diffuse beams.

We have also tried an alternative six-beam model, similar to that used by Conel,[4] in which three of the orthogonal beams are equally inclined with respect to the +x direction and the other three beams equally inclined with respect to the -x direction. This model is very convenient if the incident radiation is diffuse, but leads to difficulties for collimated incident radiation. To solve the radiative transfer problem for this orientation of the six beams one must derive coefficients S_1 and S_2 (from the single-

particle scattering coefficients) that describe respectively the

rate of scattering of the incident collimated beam into the for-

ward and backward sets of beams. In performing this calculation

we found that S_1 becomes negative if the single-particle phase

function has a sufficiently large backward-to-forward assymmetry

factor. For this reason we abandoned this model.

(2) Coarse-particle Case

In the case of coarse particles the boundary condition at the

surface of the particulate medium (x = 0) is that I(o) is matched

to the flux I_o of the incident collimated beam, while J(o) is

matched to the flux J_o of the outgoing diffuse radiation. At

x = ∞ both I and J are zero. With these boundary conditions

Equations (67) and (68) give for the reflectance J_o/I_o the ex-

pression

$$R_v = 1 + \frac{K'}{S'} - \sqrt{(\frac{K'}{S'})^2 + 2(\frac{K'}{S'})} \tag{71}$$

It is worth noting that our six-beam transfer model does

not involve a gradual conversion of the incident collimated beam

Arthur D Little, Inc.

into diffuse radiation in the medium as in the model of Duntley[19] which is similar to an earlier version of our theory. While this change made little difference,[20] our present model is much easier to apply and can readily be extended to the case of oblique incidence.

The scattering coefficients S_t and S_b in (69) and (70) are given by

$$S_t = N\ \sigma_t \tag{72}$$

$$S_b = N\ \sigma_b \tag{73}$$

Here N is the number of particles per unit volume and σ_t, σ_b are the total single-particle crosssections for transverse and backward scattering:

$$\sigma_t = \sigma_{refr,t} + \sigma_{refl,t} + \sigma_{int.refl,t} \tag{74}$$

$$\sigma_b = \sigma_{refr,b} + \sigma_{refl,b} + \sigma_{int.refl,b} \tag{75}$$

The absorption coefficient K is given by

$$K = N\ \sigma_{abs} \tag{76}$$

The particle density N is related to the particle volume-

fraction f and the diameter d of the equivalent sphere by the

formula

$$N = \frac{6f}{\pi d^3} \tag{77}$$

In the case of a mixture of particles, or of a distribution

of sizes, we attach a subscript j to f and d in (77) and sum (72),

(73) and (76) over j to obtain average values of S_t, S_b and K.

(3) Fine-Particle Case

In the case of fine particles the boundary condition at the

surface of the medium is that both the incident collimated beam

I_o and the outgoing internal beam J undergo Fresnel reflection

due to the L.L. index $\bar{m}$ of the medium. The surface reflectance

R_s is given by

$$R_s = \left| \frac{\bar{m} - 1}{\bar{m} + 1} \right|^2 \tag{78}$$

With this boundary condition the reflectance R derived from

Equations (67) and (68) now becomes

$$R = R_s + \frac{(1 - R_s)^2 R_v}{(1 - R_s R_v)} \tag{79}$$

II-38

Arthur D Little, Inc.

where R_v is the volume reflectance given as before by (71).

As in the coarse-particle case, a comment is in order here. Since our model involves only collimated rather than diffuse beams the phenomenon of trapped radiation[19] due to total internal reflection does not arise since all beams are either perpendicular or parallel to the surface of the medium.

The coefficients S_t, S_b and K for the fine-particle case are

$$S_t = \frac{4}{6} N \sigma \qquad\qquad (80)$$

$$S_b = \frac{1}{6} N \sigma \qquad\qquad (81)$$

$$K = \frac{4\pi\bar{k}}{\lambda} \qquad\qquad (82)$$

where σ is given by (58). For mixtures we again use average values of S_t, S_b and K obtained by attaching a subscript j to f and d in (77) and summing over j.

COMBINATION OF COARSE AND FINE PARTICLE THEORIES

For particles in the size range between a few tenths of a wavelength and one wavelength neither the coarse nor the fine par-

ticle theory would be expected to give accurate results. The laws

of geometrical optics used in the ray tracing part of the coarse

particle theory begin to break down for particles smaller than the

wavelength and the laws of wave optics gradually take over. Again,

for particles larger than a few tenths of a wavelength the concept

of the average L.L. index used in the fine particle theory becomes

inexact because neighboring particles are too widely spaced to

produce strong coherent scattering. Moreover, the dipole approx-

imation used in the Rayleigh scattering part of the fine-particle

theory becomes a progressively poorer approximation as the par-

ticles become larger.

It would clearly be impractical to derive a comprehensive

theory for particles of any size which would include the effects

of coherence, edges, asperities, and particle shape. Instead, we

use an empirical bridging formula that reduces to the coarse-particle

theory for large particles and to the fine-particle theory for very

small particles. The main justification for the bridging formula

is that for particles in the intermediate size range the coarse-

and fine-particle theories give calculated reflection spectra

that resemble each other.

We assume a bridging formula of the type

$$R = F\, R_{coarse} + (1 - F)\, R_{fine} \tag{83}$$

where F is a weighting factor that is a function of the size para-

meter $x = \pi d/\lambda$. A simple expression for F in terms of x that

approaches 1 when x is large and 0 when x is small is:

$$F = \frac{Ax^p}{1 + Ax^p} \tag{84}$$

where p is a positive integer and A is a parameter that determines

the suddenness of the transition from coarse-particle theory to

fine-particle theory. We have found by trial that the values

$p = 1$, $A = 6$ produce a merging of the two theories that gives

good agreement with experiment over a wide range of particle

sizes. Under these conditions (84) becomes

$$F = \frac{6x}{1 + 6x} \qquad\qquad (85)$$

COMPUTATION

The theory described above has been programmed using Fortran

IV for high speed computations. The input variables are the par-

ticle sizes, d_j, the complex refractive indices, $m_j(\lambda)$, the mineral

volume fractions, f_j and two adjustable parameters b and NV which

are involved in the effects of dipole absorption by edges and

surface asperities respectively.

The complex refractive indices are provided as needed in

the program by means of a dispersion formula containing a small

number of Lorentz resonance terms and a high frequency dielec-

tric constant. Each resonance term is defined by the usual three

classical oscillator parameters; line frequency, width and strength.

The values for the oscillator parameters are taken from published

results where available.[21,22] Otherwise we derive them ourselves

using a similar least squares method of fitting reflectance spectra,

Arthur D Little, Inc.

calculated from the dispersion formula, to the observed reflec-

tance spectra of polished samples.

In the case of uniaxial birefringent minerals, we treat

the indices for the $E \perp C$ and $E \parallel C$ orientations with suitable

weighting factors as though they represent different species.

While this is not an exact method, it has proven to be a very

satisfactory approximation.

The output of the program consists of the reflectance as

calculated by either the coarse-particle theory or the fine-particle

theory or a combination of the two theories as described above,

both in the form of printed outputs and spectral plots. The

results of a number of intermediate calculations of quantities

such as the various K's and S's are also produced and these are

very useful in developing an understanding of the complicated

processes involved.

The program which has not yet been fully optimized takes

about 1 minute for a 300 point spectrum on an IBM 360/65 machine,

for a two component mixture and single particle size. Provision

for running a particle size dispersion is provided but the running

time is not simply proportional to the number of particle sizes

employed as repetitive calculations are avoided. The times involved

in performing these calculations can thus be seen to be quite modest.

DISCUSSION AND CONCLUSION

The theory presented above contains a number of innovations

in the treatment of the interaction of radiation with a particulate

medium. As mentioned earlier, we consider that the most important

innovations are the inclusion of the additional absorption caused

by edges and asperities on coarse particles. Without allowance

for these effects one cannot achieve a good fit between theory and

experiment in the reststrahlen regions of the spectrum.

Other new features are involved in the calculation of the

single particle crosssections in the coarse-particle theory, in-

cluding the use of the Poynting vector rather than the wave normal

Arthur D Little, Inc.

in coarse particle ray tracing; the separate evaluation of the crosssections for external reflection, multiple internal reflection, and refraction, which provides considerable insight into the relative importance of the three mechanisms; and the use of the $\cos^2\phi$, $\sin^2\phi$ weighting factors to convert the single-particle phase function into the mathematically convenient form of six discrete beams.

In the fine-particle theory the recognition of the "resonances" associated with ellipsoid shape appears to be new, as well as the method of averaging over a wide range of shape, both for the Lorentz-Lorenz index and for the Rayleigh scattering. The immersed-particle model used to calculate the Rayleigh scattering of closely spaced fine particles is also novel.

The use of separate theories for coarse and fine particles along with a bridging formula for intermediate particle sizes seems to be a different approach. This method is seen to be a

necessary procedure as soon as one recognizes the essential differ-
ence between the regimes of coherent and incoherent scattering by
the particles.

Finally, the six-beam radiative transfer method, in which
the four transverse beams act as a radiation reservoir that inter-
acts with the forward and backward beams, is new and well matched
to the six-beam single-particle phase function.

The development of the theory has proceeded by a process of
successive refinement of approximations as the results of the com-
putations were compared with experimental data. A number of re-
finements remain to be made. Among the most important of these
is a suitable allowance for the fact that opaque particles in
densely packed powders shadow each other in a way not allowed for
in any continuum model. We have attempted to solve this problem
by replacing the derivatives on the left-hand sides of Equations
(59)-(64) by the finite intensity differences ΔI, ΔJ, etc., that

exist across an individual particle. On solving the difference

equations for a monolayer of particles of diameter d we find for

the reflectance and absorptance of the monolayer:

$$\rho = \left(\frac{6f}{\pi d^3}\right)^{\frac{2}{3}} \left(\frac{4 \, \sigma_{abs} \, \sigma_b + 2 \, \sigma_b \sigma_t + \sigma_t^2}{4 \, \sigma_{abs} + 2 \, \sigma_t}\right) \tag{86}$$

$$\alpha = \left(\frac{6f}{\pi d^3}\right)^{\frac{2}{3}} \left(\frac{4 \, \sigma_{abs}^2 + 6 \, \sigma_{abs} \, \sigma_t}{4 \, \sigma_{abs} + 2 \, \sigma_t}\right) \tag{87}$$

where f is the volume fraction of the particles and σ_{abs}, σ_t, σ_b

are given, as before, by (17), (74), and (75). The reflectance

of a semi-infinite stack of monolayers is

$$R_v = \left(\frac{1 + \rho^2 - \tau^2}{2\rho}\right) - \left\{\left(\frac{1 + \rho^2 - \tau^2}{2\rho}\right)^2 - 1\right\}^{\frac{1}{2}} \tag{88}$$

where τ, the monolayer transmittance, is given by

$$\tau = 1 - \rho - \alpha \tag{89}$$

A comparison of spectral reflectances calculated by the non-

continuum formula (88) and the continuum formula (71) shows that

the non-continuum model gives significantly higher reflectance in

Arthur D. Little, Inc.

strong reststrahlen regions and is thereby in better agreement with

experimental spectra. As one would expect, the two theories give

identical results in regions of the spectrum where ρ and $1-\tau$ are

small. Unfortunately, the non-continuum model, like that of

Melamed,[11] cannot be easily extended to the important case of a

medium composed of a mixture of particles of different materials

with a wide range of sizes, such as occurs on planetary-surfaces.

The present continuum model, on the other hand, is able to treat

such a medium, although with some loss of accuracy in the general

spectral level.

An assumption in the coarse-particle theory is that the rays

enter each material from the void rather than directly from one

material into another. While this is a good approximation for

relatively low density powders, it will break down in the case of

compact agglomerates. In principle we could extend the computa-

tional techniques to handle this case. Another difficult case

would be the suspension of coarse particles of some materials in

a medium composed principally of fine-particles of other materials.

The present theory is capable of treating this case as well, again

with some modifications of the computer programs.

We intend to apply the theory described in this paper to

transmission spectra of atmospheric clouds and aerosols in the

near future. In the aerosol case immersed-particle scattering

reduces to ordinary Rayleigh scattering owing to the small volume

fraction of the fine particles involved.

Our method of separately calculating the various scattering

crosssections of a single particle allows relatively simple modi-

fications of the crosssection formulas to be made, so that one can

treat the case of particles of non-spherical gross shape, e.g.,

platelets or cylinders. Such particles are often encountered in

ice-crystal clouds. It is to be noted that thin platelets give

little refractive scattering although in any theory based on a

spherical model (e.g. Mie theory) a refractive contribution is

automatically included.

ACKNOWLEDGMENT

Arthur D Little, Inc.

REFERENCES

1. _Modern Aspects of Reflectance Spectroscopy_, W.W. Wendlandt,

   Ed., Plenum Press, New York, 1968.

2. W.W. Wendlandt and H.G. Hecht,"Reflectance Spectroscopy",

   Interscience Publishers, New York, 1966, chIII.

3. G. Mie, Ann. Phys. $\underline{25}$, 377 (1908).

4. J.E. Conel, J.Geophys. Res. $\underline{74}$, 1614 (1969).

5. A. Schuster, Astrophys. J. $\underline{21}$, 1 (1905).

6. P. Kubelka and F. Munk, Z. Techn Physik $\underline{12}$, 593 (1931).

7. S. Chandrasekhar, "Radiative Transfer", Clarendon Press,

   Oxford, 1950 (Reprinted by Dover Publications, Inc.,

   New York, 1960).

8. G.N. Plass and G.W.Kattawar, J. Atm. Sci. $\underline{28}$, 1187 (1971).

8. G.N. Plass and G.W. Kattawar, Appl. Opt. $\underline{7}$, 415 (1968).

8. G.N. Plass and G.W. Kattawar, Appl. Opt. $\underline{7}$, 699 (1968).

9. W.R. Blevin and W.J. Brown, J. Opt. Soc. Am. $\underline{51}$, 129 (1961).

10. A.L. Lathrop, J. Opt. Soc. Am. <u>56</u>, 926 (1966).

11. N.T. Melamed, J. Appl. Phys. <u>34</u>, 560 (1963).

12. J.R. Aronson and A.G. Emslie, Appl. Opt. __ (1973).

13. C.S. Strachan, Proc. Cambridge Phil. Soc. <u>29</u>, 116, (1933).

14. D.W. Berreman, J. Opt. Soc. Am. <u>60</u>, 499, (1970).

15. J.R. Aronson, A.G. Emslie and H.G. McLinden, Science <u>152</u>, 345 (1966).

16. A.G. Emslie, "Theory of Diffuse Spectral Reflectance of a Thick Layer of Absorbing and Scattering Particles", in <u>Progress in Astronautics and Aeronautics Vol. 18</u>, G.B. Heller, Ed., Academic Press, New York, 1966.

17. J.R. Aronson, A.G. Emslie, R.V. Allen and H.G. McLinden, J. Geophys. Res. <u>72</u>, 687 (1967).

18. H.C. van de Hulst, "Light Scattering by Small Particles", John Wiley and Sons, New York, 1957, p-64.

19. S.Q. Duntley, J. Opt. Soc. Am. <u>32</u>, 61 (1942).

20. J.R. Aronson and A.G. Emslie, The Moon, $\underline{5}$, 3 (1972).

21. W.G. Spitzer and D.A. Kleinman, Phys. Rev. $\underline{121}$, 1324 (1961).

22. A.S. Barker, Jr., Phys. Rev. $\underline{132}$, 1474 (1963).

III. The Spectral Reflectance and Emittance
of Particulate Materials,

Part II Application and Results

J. R. Aronson and A. G. Emslie
Arthur D. Little, Inc.
Cambridge, Massachusetts   02140

Abstract

Experimental data on the spectral emittance of particulate minerals, obtained using a Michelson Interferometer operating between 300 and 1400 cm^{-1} are compared with the results of a new theory of the spectral reflectance (emittance) of such materials. The comparisons show that the theory predicts the infrared spectra of minerals quite well both for single substances and mixtures, over the wide particle size range between 0.3μ and 330μ. The good agreement suggests that the theory can be used in the application of remote infrared spectroscopy to such problems as the compositional analysis of the surface of a planet.

INTRODUCTION

For many years it has been recognized that infrared spectroscopy provides unique information as to the composition of minerals. This results from the rich vibrational spectra that may be obtained in the infrared region. While most workers have concentrated their efforts on laboratory transmission spectra, such

Arthur D Little, Inc.

potentially important remote sensing techniques as emission and reflection were in fact investigated by Coblentz [1] almost three quarters of a century ago. The advent of the space program re-awakened an interest in this topic and a number of groups proposed remote infrared spectroscopy as a very valuable tool for the evaluation of planetary surface mineralogy from orbiting or flyby spacecraft. The instrumental capability for obtaining excellent remote data has continued to improve as is demonstrated by recent results from the Mariner Mars [2] and Nimbus [3] orbiting spacecraft.

While the reflectance spectra of polished mineral samples provide many strong features suitable for relatively simple interpretation, the spectra of roughened or particulate samples change in important ways with the degree of roughness or the particle size and packing density. For some time, it was be-lieved by many investigators that the spectra of finely divided minerals approximate blackbody spectra and thus contain very little or no information as to composition. We showed[4] both experimentally and theoretically that this was not true but that the problem was simply one of the signal-to-noise ratio. Others[5,6] examined the effects of particle size on spectral shape and found that different spectral features had widely differing behaviors as a function of particle size. In some cases[7] peaks could even turn into troughs. As the greatest difficulties inherent in the prospects for remote mineral analysis by infrared spectroscopy were clearly those of

Arthur D Little, Inc

interpretation, we began the development of a new theory of the reflectance or emittance of particulate solids several years ago[8]. The current status of the theory is detailed in the preceding paper[9] (hereafter referred to as I).

An earlier version of the theory produced relatively good agreement with experimental data [10] in the coarse-particle regime. The agreement in all particle size ranges has continued to improve through a process of successive refinement of the assumptions as discrepancies appeared in the comparison of theoretical predictions with experimental measurements.

APPARATUS

Our measurements have been made on a 7–35μ (1400–300 cm^{-1}) Michelson interferometer spectrometer system, which uses a germanium coated CsI beamsplitter and a Barnes TGS pyroelectric detector. Figure 1 shows the Interferometer. Figure 2 shows the sample chamber in which the emittance spectra of mineral powders and comparison blackbody sources are measured. The samples are heated from below and mounted on a lazy susan turntable so that alternate measurements can be made without breaking the vacuum or inert gas atmosphere. Vacuum measurements can be made to investigate the effects of high thermal gradients on the spectra. Figure 3 shows the entire system including a digital data acquisition system based on a Hewlett-Packard 2116B minicomputer.

The powders are generally supported in a sample tray 0.6 cm deep with a total volume of 3.04 cm^3. This tray is instrumented
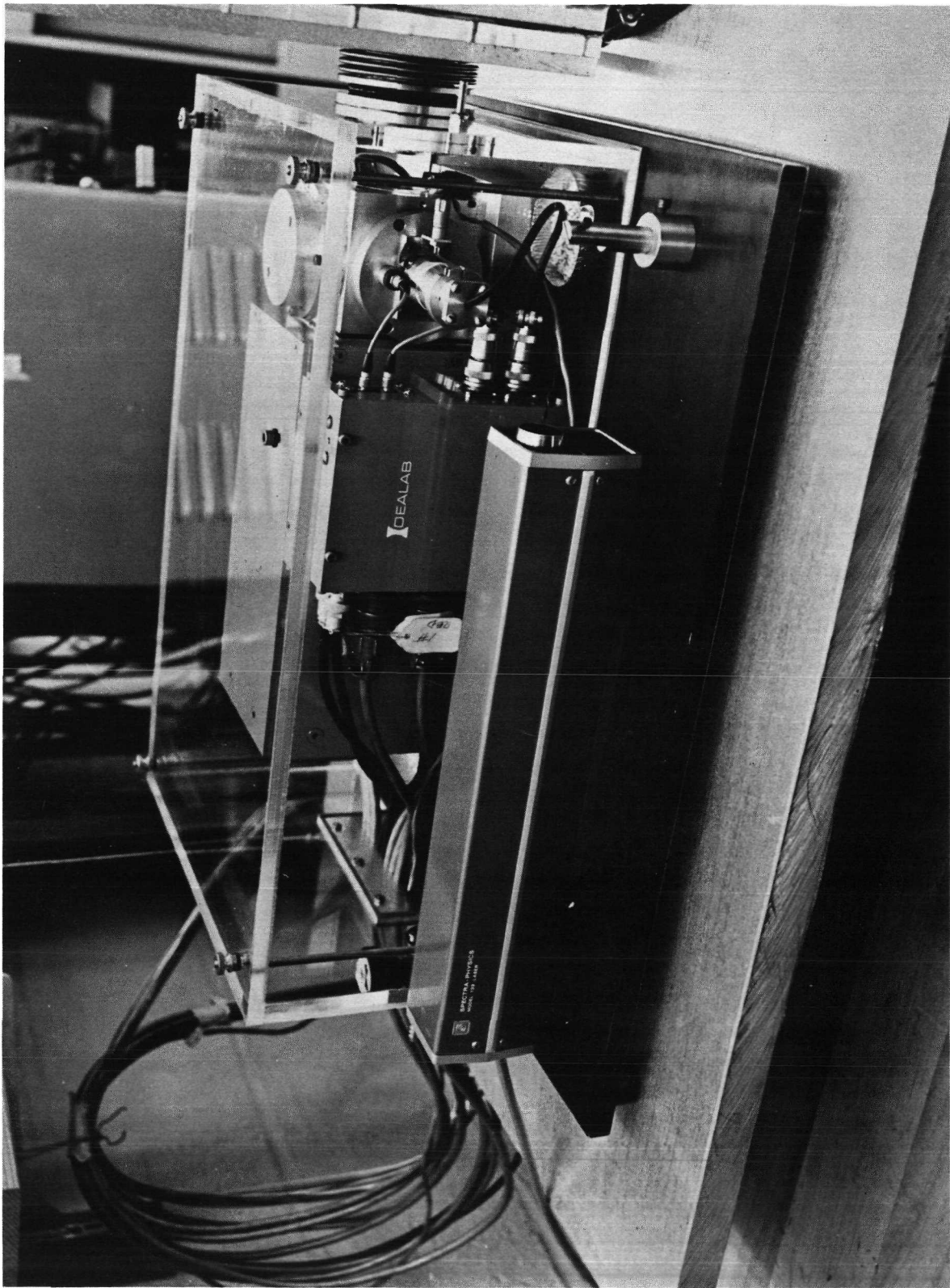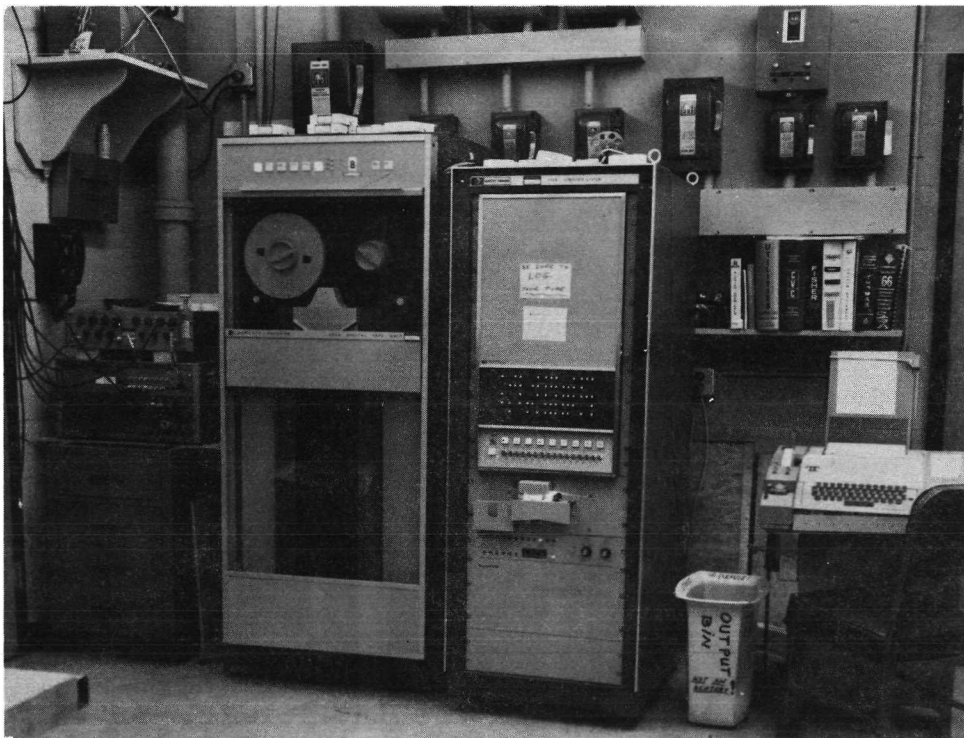
FIGURE 1 · MICHELSON INTERFEROMETER

Arthur D. Little, Inc.
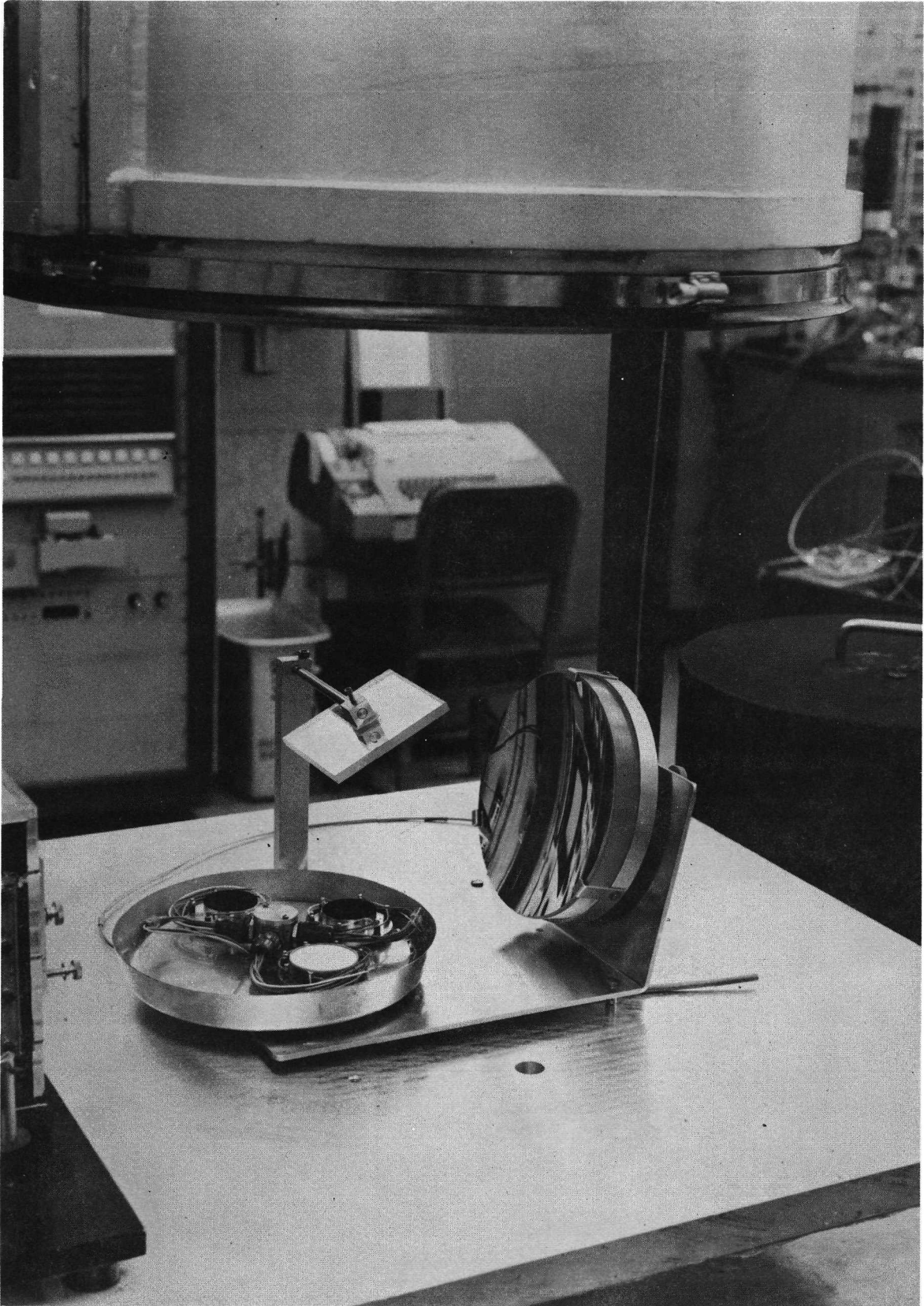
FIGURE 2   EMITTANCE OPTICS

III-5

FIGURE 3 INTERFEROMETER SYSTEM

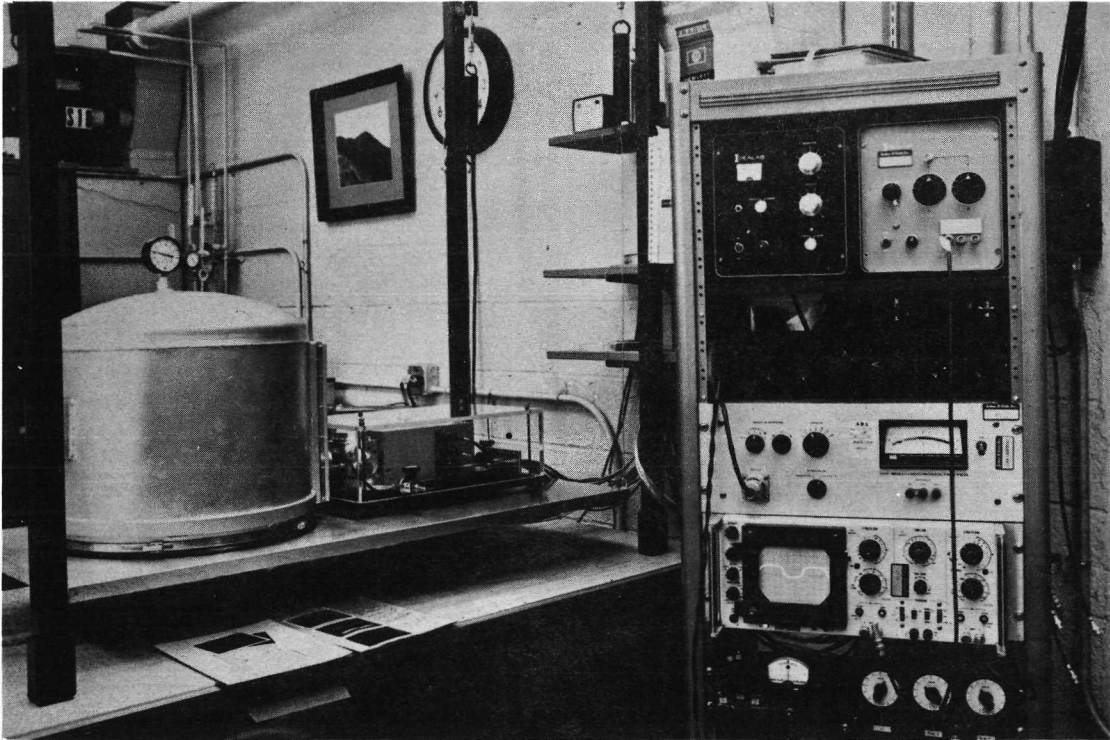Arthur D. Little, Inc.

for temperature measurements by imbedding a thermistor in the base and stringing two sets of 0.05 cm differential copper-constantan thermocouples 0.2 and 0.5 cm above the base (Figure 4). The gradient between the upper two stations is extrapolated to the nominal surface in order to provide a first estimate of the "surface" temperature. Thermistors located on the interferometer detector case, on the black shield that surrounds the sample chamber, and on the experimental blackbodies provide the other temperatures required for data reduction.

The experimental blackbodies are constructed of aluminum and have concentric 30° V-grooves cut into the surface. They are coated with Parsons black paint (Eppley Laboratory) as previous results using Nextel black paint (Minnesota Mining and Manufacturing Co.) indicated the presence of spectral features near 1090 cm^{-1} and 460 cm^{-1}, owing to the presence of small glass beads in the Nextel paint. The Parsons black standard was run against a Cabot Corporation Carbolac-1 black powder sample (9m μ carbon particles) as well as a Nextel-coated standard and the data indicate a spectrally flat emittance for the Parsons standard from 1400 cm^{-1} to about 500 cm^{-1}. The emittance of the Parsons standard then appears to fall monotonically reaching apparent values of about .97 near 350 cm^{-1}.

DATA REDUCTION

The data reduction procedure involves Fourier transformation of the interferograms of the sample and the two experimental
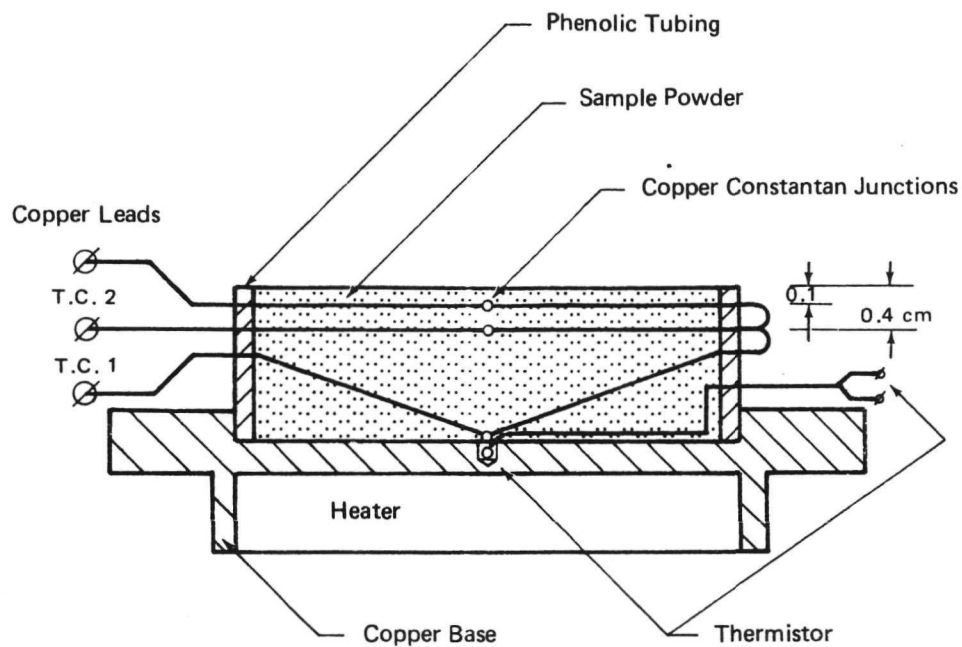
Arthur D. Little, Inc.

FIGURE 4   SAMPLE TRAY (not to scale)

blackbodies which are run at temperatures close to that of the sample and differ by about 5°C. High signal-to-noise data are obtained with a sample surface temperature about 15°C above the near-ambient interferometer and shield temperatures in about 20 minutes with a spectral resolution of about 3 cm^{-1}.

The spectral emittance $\varepsilon_s(\nu)$ of the sample is the spectral radiance $N_s(\nu)$ of the sample divided by the spectral radiance $B_s(\nu)$ of a blackbody at the same temperature as the sample. We calculate $B_s(\nu)$ from the Planck function using the inferred surface temperature of the sample. We determine $N_s(\nu)$ from the measured output spectrum $E_s(\nu)$ of the sample by means of the instrument transfer function and a correction for radiation from the shield that is reflected from the sample.

The transfer function relates radiance $N(\nu)$ to spectral output voltage $E(\nu)$ obtained by Fourier transformation of the interferogram. We assume that the formula is linear and of the form

$$N = N_o + \frac{E}{R} \tag{1}$$

where N_o, the input radiance that produces zero output signal, is equal to the radiance of the instrument in the direction towards the sample. To determine N_o and R we replace the sample successively by two blackbodies at temperatures T_1 and T_2. Then, from (1)

$$\varepsilon_1 B_1 = N_o + \frac{E_1}{R} \tag{2}$$

Arthur D Little, Inc.

$$\varepsilon_2 \, B_2 = N_o + \frac{E_2}{R} \tag{3}$$

where ε_1, ε_2 are the emittances of the "blackbodies," which would allow for small departures from perfect blackbody behavior.

From (2) and (3) we obtain for $R(\nu)$ and $N_o(\nu)$:

$$R(\nu) = \frac{E_1 - E_2}{\varepsilon_1 \, B_1 - \varepsilon_2 \, B_2} \tag{4}$$

and

$$N_o(\nu) = \frac{1}{2} \left[\varepsilon_1 \, B_1 + \varepsilon_2 \, B_2 - \frac{1}{R} (E_1 + E_2) \right] \tag{5}$$

With the sample in place we determine the net radiance N_s of the sample from the measured spectral output E_s by means of Eq (1)

$$N_s = N_o + \frac{E_s}{R} \tag{6}$$

and where R and N_o are known from (4) and (5).
On combining (4) – (6) we can express N_s directly in terms of the measured quantities E_1, E_2 and E_s:

$$N_s = \frac{1}{2} (\varepsilon_1 B_1 + \varepsilon_2 B_2) + \frac{1}{2} (\varepsilon_1 B_1 - \varepsilon_2 B_2) \left(\frac{2E_s - E_1 - E_2}{E_1 - E_2} \right) \tag{7}$$

Finally, the emittance ε_s of the sample is computed from the formula

$$\varepsilon_s = \frac{N_s - B_c (1 - \frac{\Omega}{\pi}) - B_i \frac{\Omega}{\pi}}{B_s - B_c (1 - \frac{\Omega}{\pi}) - B_i \frac{\Omega}{\pi}} \tag{8}$$

which is based on simple radiative transfer considerations. Here B_c is the radiance of the cavity or shield (assumed to be a blackbody) at temperature T_c surrounding the sample, B_i is the

III-10

radiance of the interferometer aperture (also assumed to be a black-body at temperature T_i), B_s is the Planck function for the temperature T_s of the sample, and Ω is the solid angle subtended at the sample by the interferometer aperture. The cavity walls are coated with 3M Nextel black paint which, together with multiple reflections, should make it an almost perfect blackbody. In the data reduction up to the present we have assumed that the blackbodies are indeed black, so that $\varepsilon_1 = \varepsilon_2 = 1$.

As the surface of the powder cannot be microscopically smooth (we draw a spatula edge across the powder surface to prevent gross roughness) and as the depth of origin of the radiation is a function of the optical constants at the various frequencies, we cannot expect the definition of the surface to be very exact. Further, the position of the stretched thermocouple wires has some error and the possibility of a poor equilibrium between the radiation field and the shiny thermocouples is quite likely.

For all of these reasons we chose to estimate our "surface" temperature by a radiative expedient based on what is generally known as the principal Christiansen frequency[11,12]. When the refractive index, n of a substance approaches unity and the absorption index, k is quite small ($\lesssim 10^{-2}$) the amount of surface reflection is negligible and the refractive scattering is minimal. Thus the emittance is maximum and close to unity. This combination of the optical constants occurs at slightly higher frequencies than the first principal reststrahlen band.

Arthur D Little, Inc.

It cannot in principle occur for a mixture of materials as the location of the Christiansen frequency will be different for each species. Even two orientations of birefringent minerals have slightly different Christiansen frequencies. We take the value for the average of the two orientations of corundum to be 1020 cm^{-1} and for quartz to be 1360 cm^{-1} from data of Barker[13] and Spitzer and Kleinman[14]. We assume that the only significant temperature error in our data reduction scheme is that of the "surface temperature". We then use the extrapolated "surface temperature" as a first estimate of the true surface temperature and calculate an emittance spectrum. The computer program is constructed so that this temperature may be varied and the procedure is to make the required changes in this temperature so as to provide a unit emittance at the principal Christiansen frequency.

We have found that the extrapolated surface temperature and the temperature derived by the Christiansen frequency technique differ by a few tenths of a degree in cases of relatively low temperature gradients (ca. 5°/cm to 10°/cm as measured by our upper differential thermocouple) which occur in atmospheric pressure runs. Under conditions of high temperature gradients (vacuum) the procedure is quite inaccurate and we plan to discuss this in a future communication. All of the data are plotted as reflectance ($R = 1 - \epsilon$) for convenience in comparison with the theory. The validity of this procedure which is simply an application of Kirchhoff's Law for "infinitely" thick media has been previously shown[11].

COMPARISON OF THEORY AND EXPERIMENT

As discussed in (I), our theory consists of two subtheories. The first, which is based on geometrical optics supplemented by certain wave optics considerations, is applicable in the coarse-particle region which extends down to particle sizes roughly comparable with the free space radiation wavelength. The second, a fine-particle theory, is based on the Lorentz-Lorenz theory of dielectrics, and Rayleigh scattering by particles immersed in the medium whose optical properties are set by the Lorentz-Lorenz field. In order to bridge the two theories for those particle sizes falling in the ill-defined region between the regions of clear applicability of either theory, we have at present resorted to a simple empirical bridging formula that gradually merges the results of the two subtheories.

Figure 5 shows a comparison of the experimental and theoretical results for corundum powders. The 120μ sample was obtained from the Norton Company, the 0.3μ sample from Adolf Meller Co., and the other samples are LWA powders obtained from the Microabrasives Corporation of Westfield, Massachusetts. The particle sizes shown on the figure for the LWA powders are Microabrasives designations except for the 3.5μ sample. This is Microabrasives LWA 3 but our particle size counts indicated a value of about 3.8μ. The shape of the spectrum between 630 and 900 cm^{-1} and the particle size effect in regions of the spectrum where the particles are opaque was correctly predicted
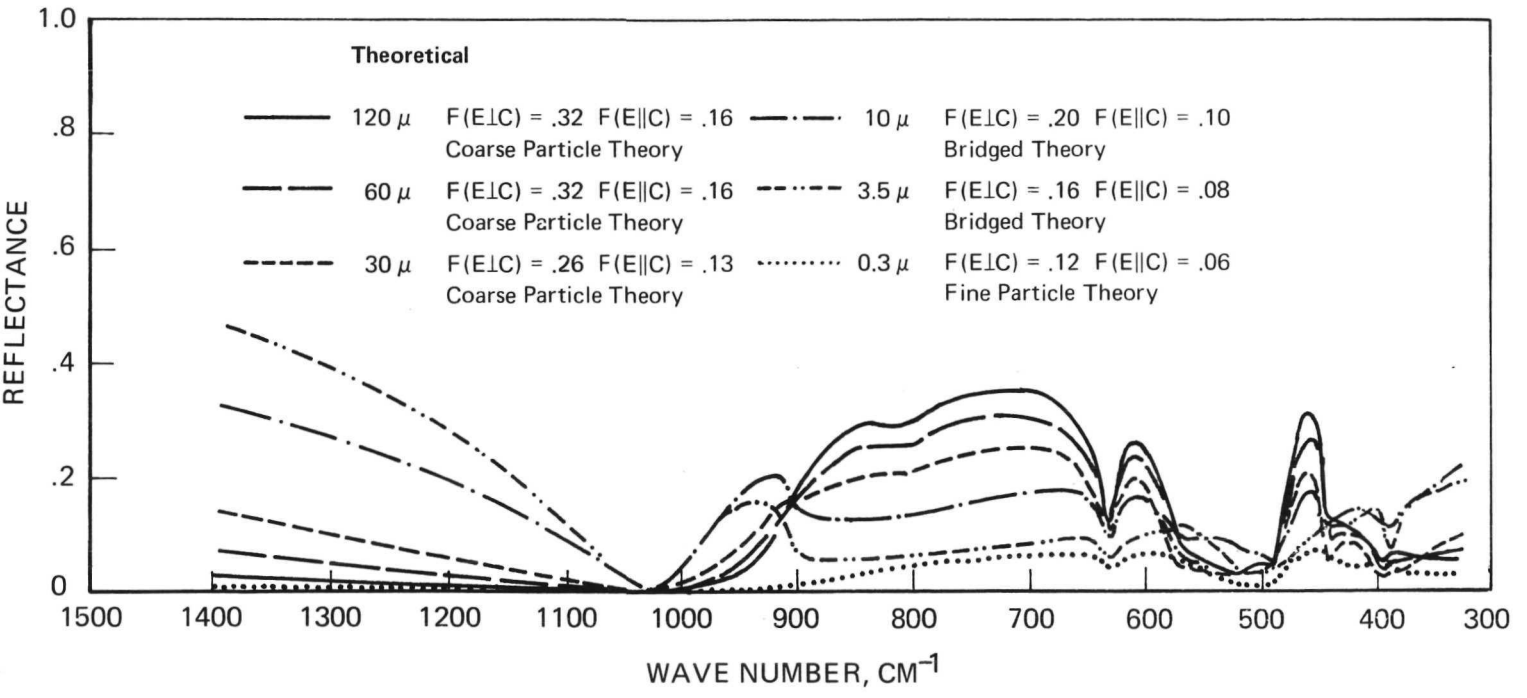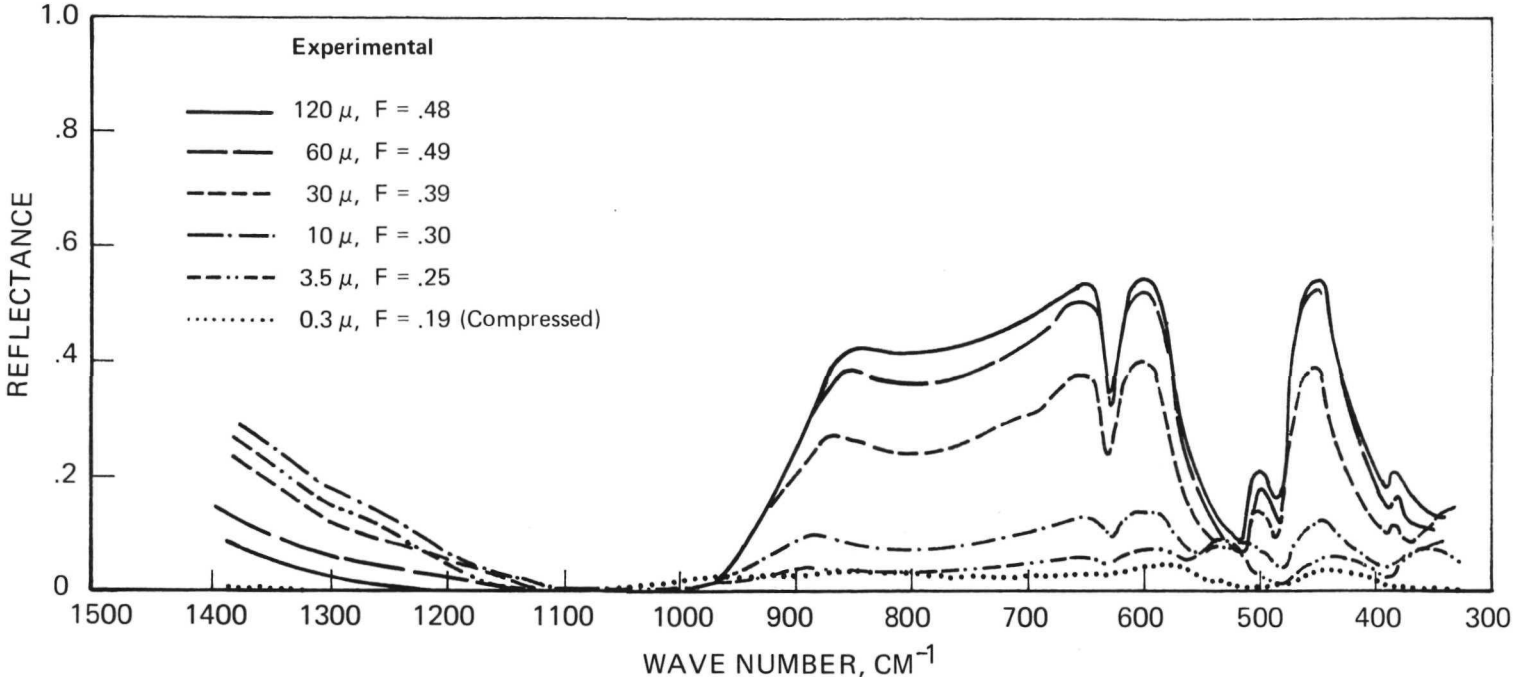
FIGURE 5   COMPARISON OF THEORETICAL AND EXPERIMENTAL REFLECTANCE OF CORUNDUM POWDERS

Arthur D Little, Inc.

only after we included the wave optics additions to the basic
geometrical optics model to account for the effects of particle
edges[10] and surface asperities. The edge effect which dominates
at the lower particle sizes (d's) of the coarse-particle theory pro-
duces the 1/d dependence of the reflectance spectra in this
region of high absorption by the particles. The fact that the
$630 - 900 \text{ cm}^{-1}$ feature persists to relatively large particle
sizes (120μ) was explicable only after scanning electron micro-
graphs (Figure 6) revealed the presence of small step-like
surface asperities for this material. If the number of these
asperities is proportional to the surface area of the particles
they will produce no d-dependent effect (see Figure 7). The
surface density of these asperities is an adjustable parameter
in the theory. The scale factor for the 1/d effect of the
particle edges has been chosen, as discussed in (I), by means of
reasonable, but somewhat arbitrary physical assumptions. We have
used the same factor for all jagged particles. The general level
observed in the reststrahlen regions for large particles in all
of our work is higher than predicted by the theory. We believe
this to be the result of deficiencies in our continuum-type
radiative transfer model as the particles in such regions are
highly opaque and therefore give rise to a large change in the
radiative fluxes in a single layer of particles, which violates
the assumptions of continuum model. Correction of the theory by
means of a discrete layer model is required.

Arthur D Little, Inc.
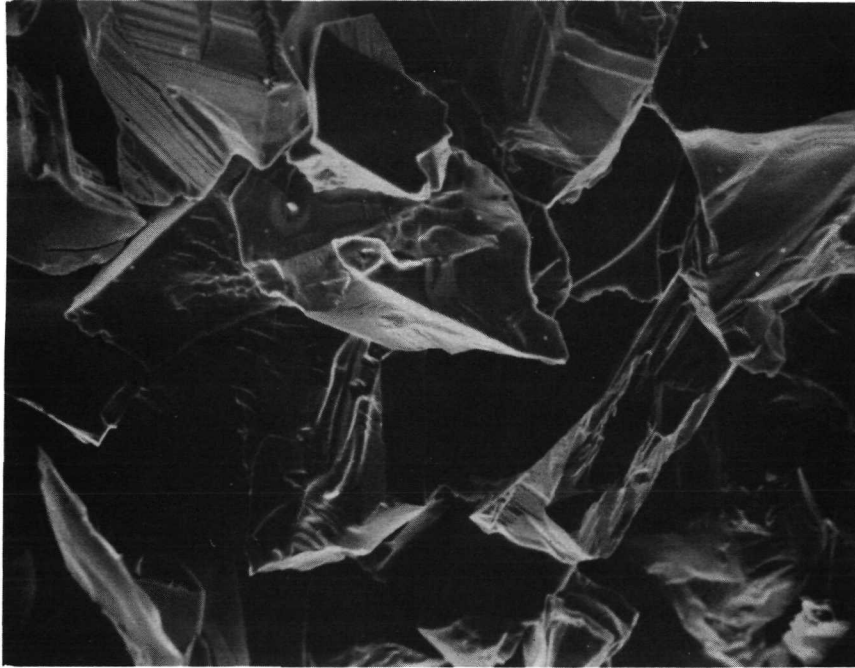
a. **SCANNING ELECTRON MICROGRAPH OF STEPLIKE ASPERITIES.
30μ CORUNDUM, 1000X**
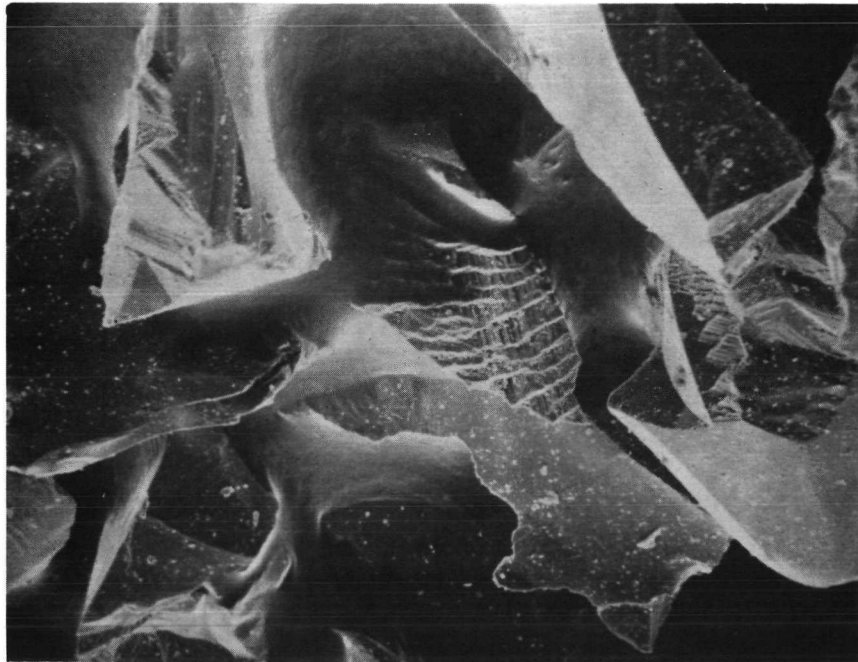
b. **SCANNING ELECTRON MICROGRAPH OF STEPLIKE ASPERITIES
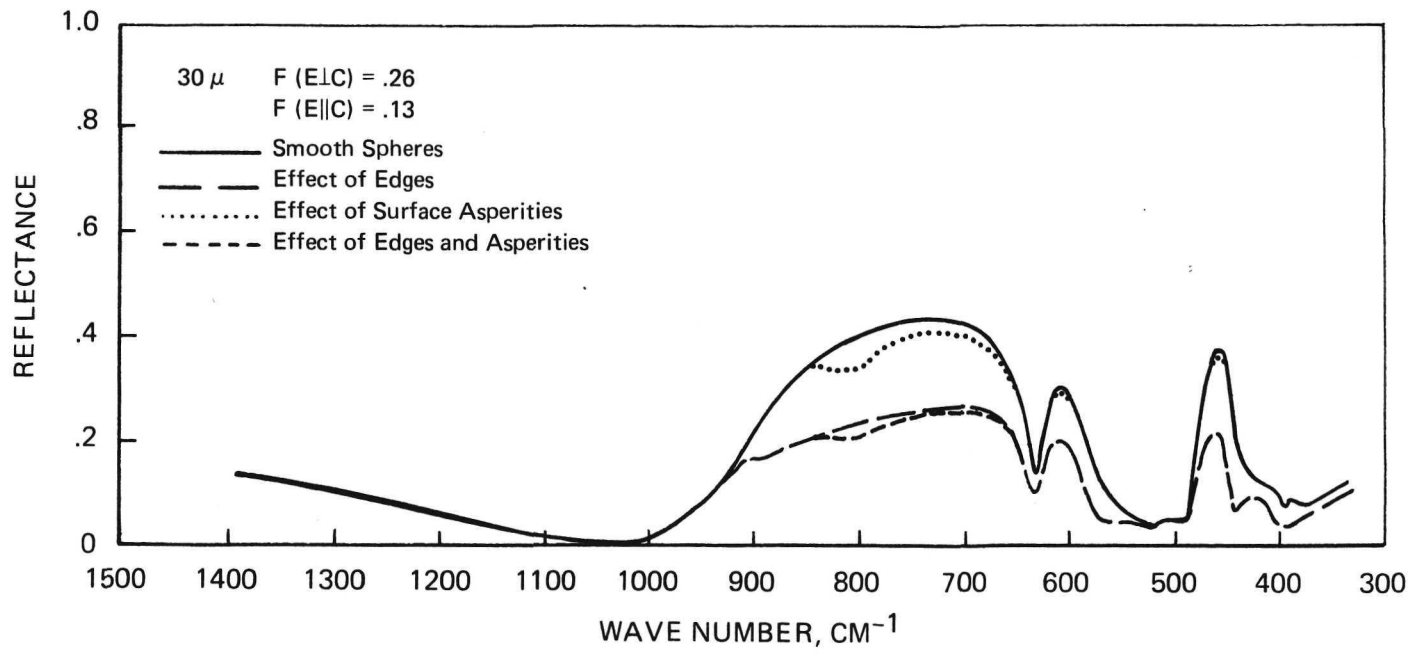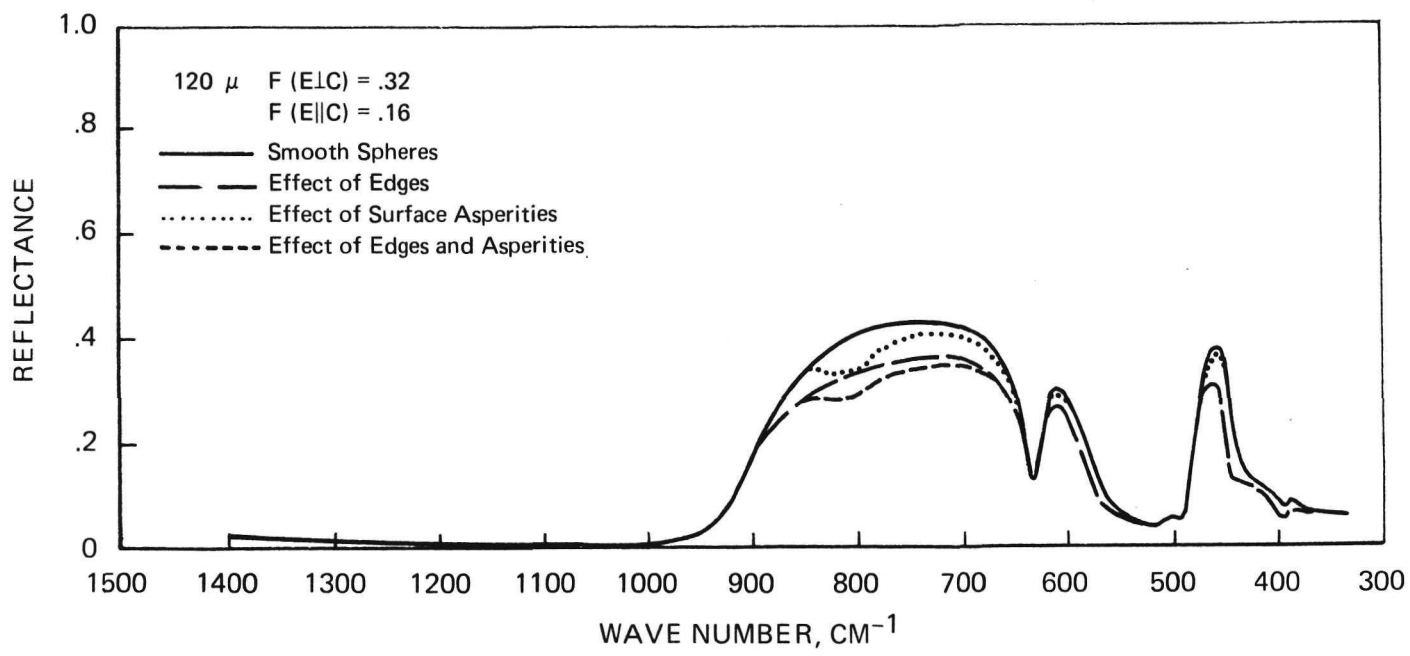AND ADDITIONAL FINES. 120μ CORUNDUM, 500X**

FIGURE 6

III-16

Arthur D Little, Inc.

FIGURE 7   THEORETICAL SPECTRA OF CORUNDUM POWDERS DEMONSTRATING THE EFFECTS OF EDGES AND SURFACE ASPERITIES

Arthur D Little, Inc.

As reduction of particle size generally results in increasing
porosity (decreased packing density) and the fine-particle theory
shows a decided porosity dependent effect owing to the dilution
of the optical constants by high void fractions, we have carried
out several experiments with the 0.3μ powder as a function of
packing density. The results showed that as packing density is
increased, the principal effect is to increase the spectral contrast
in the two features at 450 cm^{-1} and 580 cm^{-1}. The data shown
in Figure 5 for the 0.3μ sample were obtained by compressing
it gently, thus increasing the volume fraction of material to
0.19 from 0.09 which is its state as prepared by our usual
techniques.

The feature observed near 930 cm^{-1} in the theoretical
spectra for the 3.5μ and 10μ cases would be considerably reduced
if a particle size distribution had been used. It is to be noted
that the peak in the experimental spectrum in this general region
shifts to higher frequencies as the average particle size is
reduced. This may very well be the effect of a contribution by
the feature in question. The feature is caused by the onset of
a refractive contribution to the scattering as the particles
become more transparent for frequencies approaching the Christian-
sen frequency at 1020 cm^{-1}. This contribution falls off rapidly
as the frequency approaches still closer to Christiansen point.
A similar explanation applies to the theoretically predicted
convex shape of the spectra at frequencies above 1020 cm^{-1} con-
trasted with the concave shape shown by the experimental data.

Arthur D Little, Inc.

Figure 7 shows the theoretical corundum spectra as calculated for the 120μ and 30μ particle sizes by options in our program that either, 1) treat the particles as smooth spheres, 2) include both the effects of edges and surface asperities, 3) include edges, but no asperities, and 4) include asperities but no edges. As can be seen both edges and asperities are necessary to account for the particle size dependence in the reststrahlen regions and the shape of the $630 - 900$ cm^{-1} feature in the 120μ particle size sample. The amount of surface asperities used for these plots is NV = 3×10^{-7} cm (see I). This value, which corresponds to the "average" thickness of the asperity layer, indicates that a substantial change in reflectance is caused by a relatively small amount of these asperities. The effect is due to the high efficiency of absorption by ellipsoidal particles having n<<1 and k∿1 such as occur in reststrahlen bands. The amount of asperities appears compatible with photomicrographs of the particles. In a similar fashion the scale factor for the d dependence described in (I) by the value b∿λ/4π is somewhat arbitrary and might be slightly adjusted for a better fit to the data. At the present time b = 0.9 is used for all of our theoretical computations. However, as these factors are unlikely to be known precisely for arbitrary unknown samples, we have not yet optimized the fit.

The phenomenon of additional absorption by the needle-like dipoles that represent the edges and the more general spheroidal

Arthur D Little, Inc.

dipoles that represent surface asperities was an important inno-
vation in our coarse-particle theory. We therefore attempted to
prove the reality of these effects by carrying out several
critical experiments. The first of these was a comparison of a
single crystal emittance spectrum of "randomly oriented sapphire"
with the emittance spectrum obtained after substantial surface
abrasion with 15μ diamond paste. The results are shown in
Figure 8 and a stereo pair of scanning electron micrographs of
a replica of the surface are shown in Figure 9. Figure 8 shows
that the anomalous shape of the powder spectrum in the 630 -
900 cm^{-1} region can be produced in a single crystal spectrum by
providing surface asperities.

The second critical experiment was carried out by running
two samples of corundum beads (Figure 10). These beads were
produced for us by D. Spooner and R. Bechtold of the Lockheed
Electronics Geophysics section. The mechanism of bead production
is to feed small particles of corundum into a hydrogen-oxygen
flame where partial melting occurs. After air cooling, small
amounts of a number of other Al_2O_3 phases were observed by
X-ray diffraction, but annealing at 1400°C for more than 4 hours
removed the other phases, resulting in pure α-Al_2O_3. Figure 11
shows scanning electron micrographs of the sapphire beads. Sur-
face asperities similar to those shown for most samples of
crushed corundum (Figure 6) still occur on these beads. Some
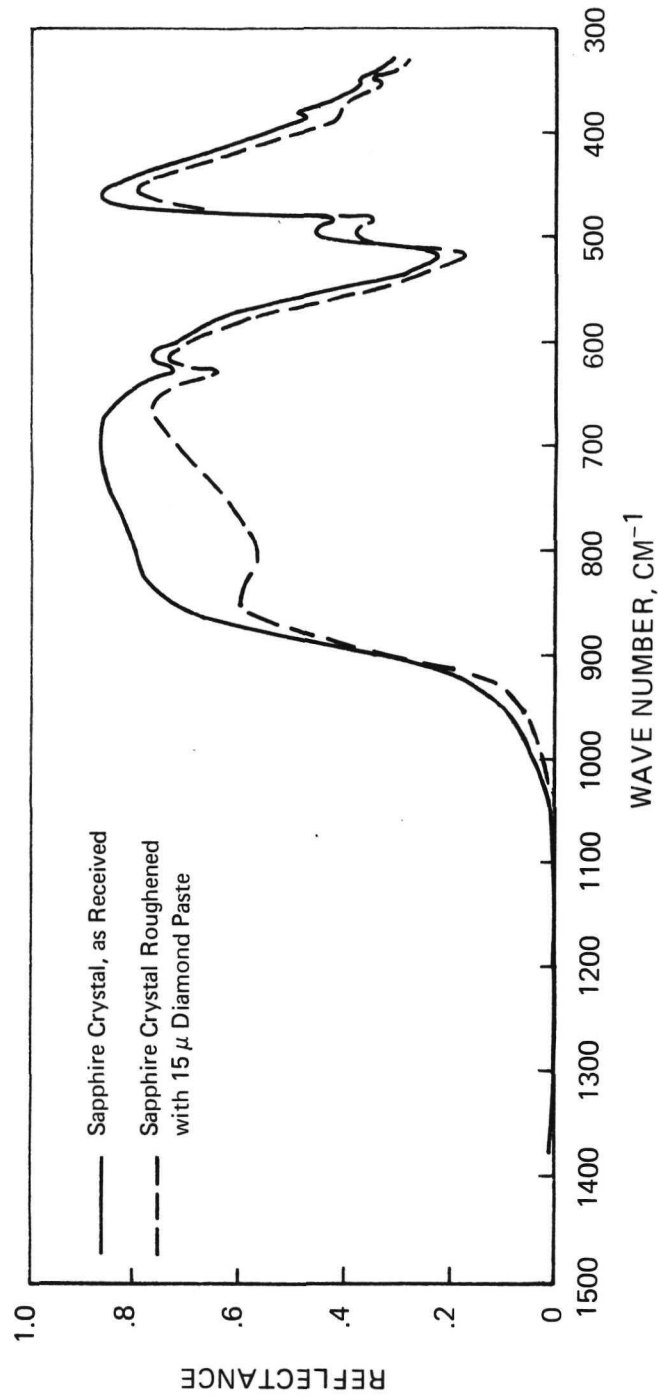non-spheroidized material still exists, principally in the smaller

FIGURE 8   EXPERIMENTAL RESULTS OF ABRADING SAPPHIRE
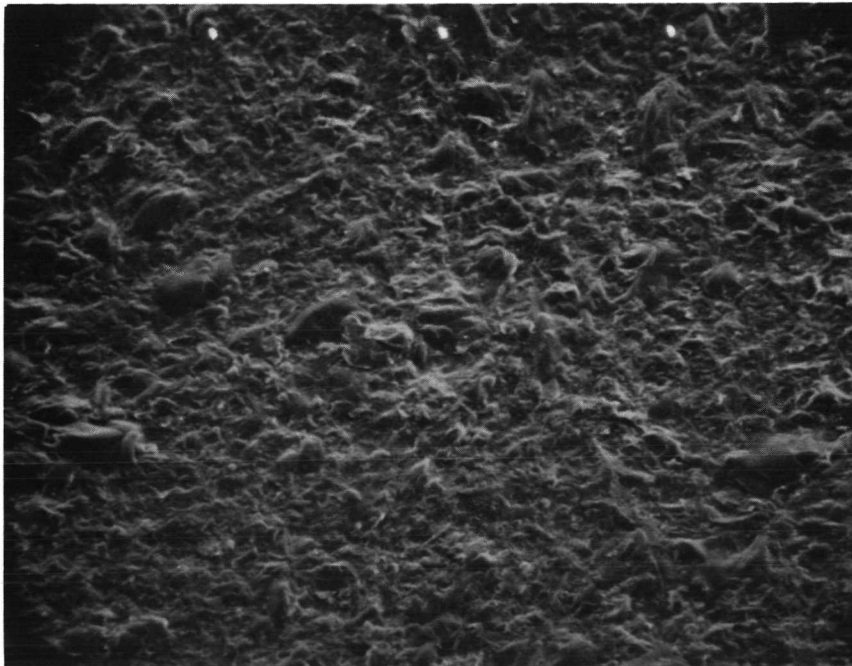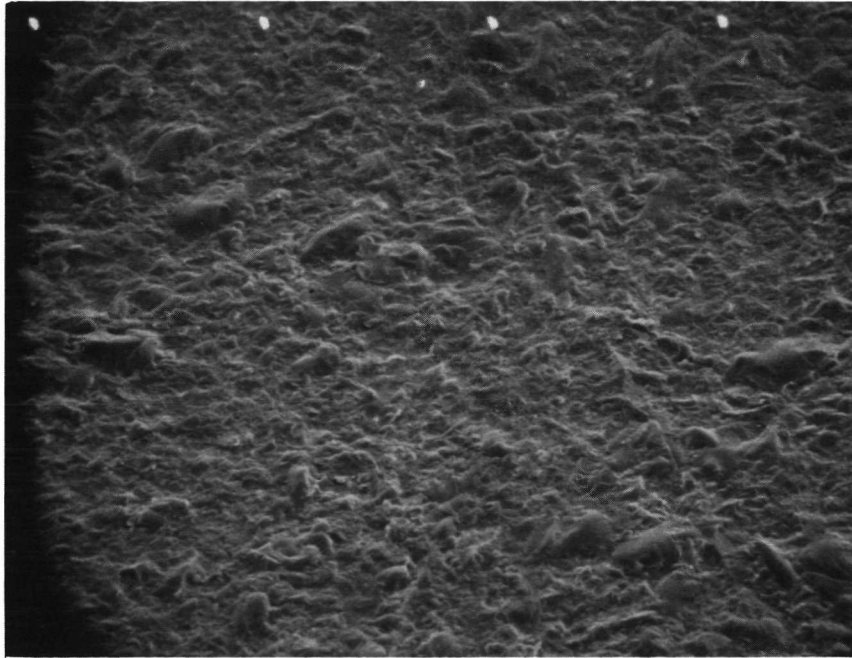
III-21

FIGURE 9   SCANNING ELECTRON MICROGRAPHS OF REPLICA OF ABRADED SAPPHIRE CRYSTAL. PHOTOGRAPHS ROTATED TO SIMULATE THE ACTUAL SURFACE (470X).

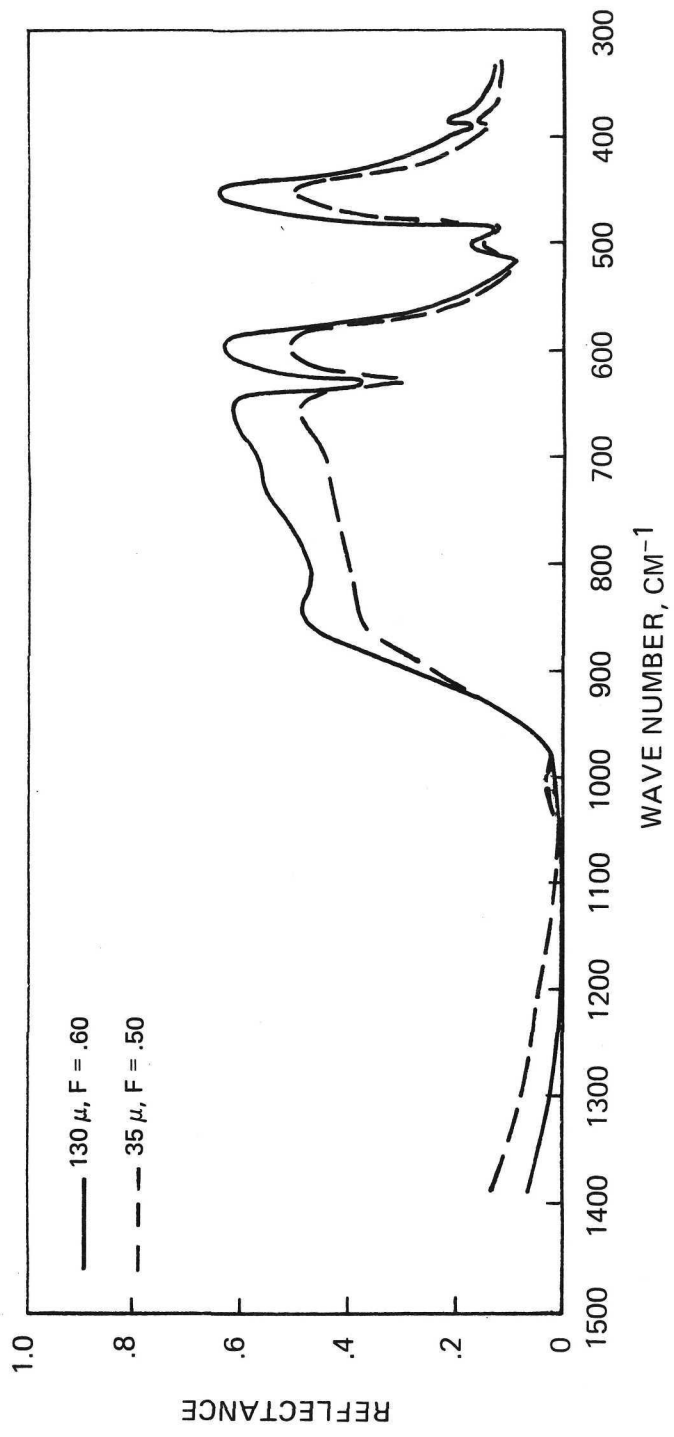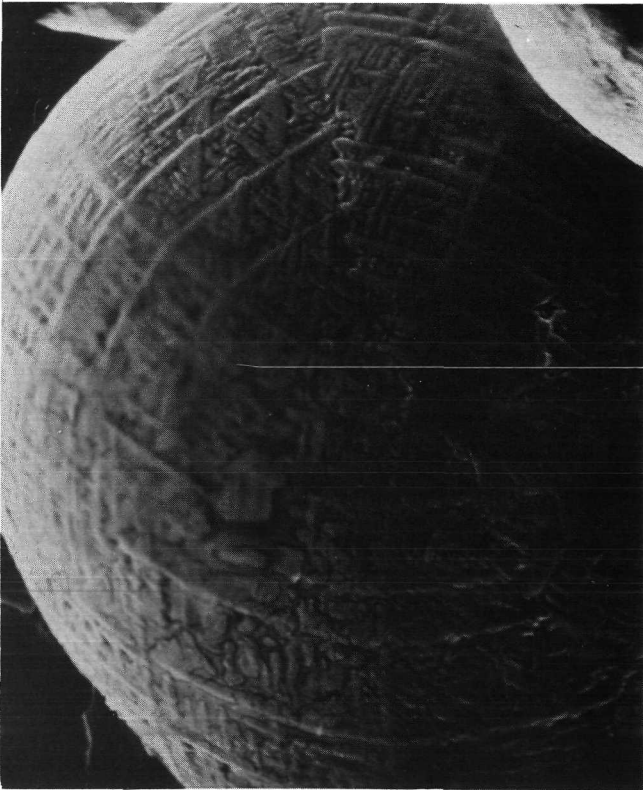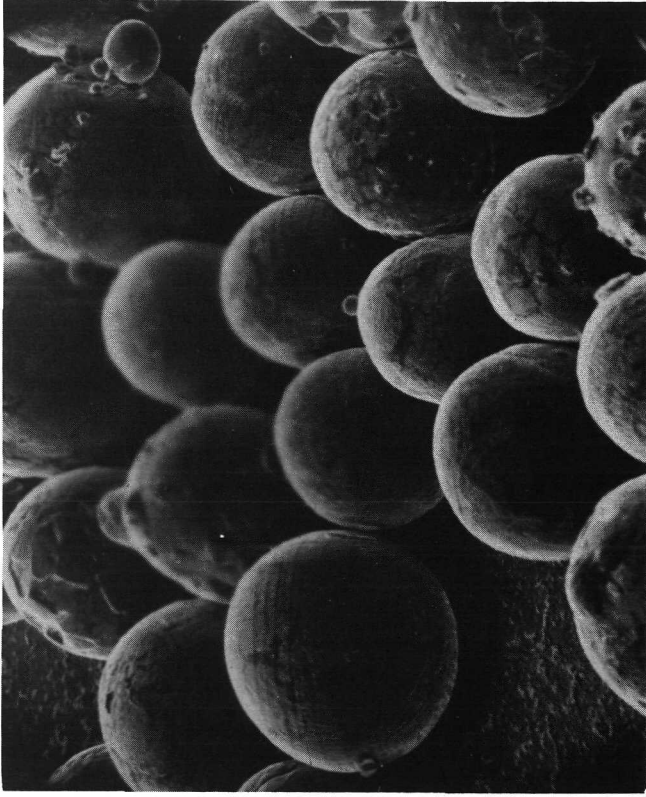Arthur D Little, Inc.

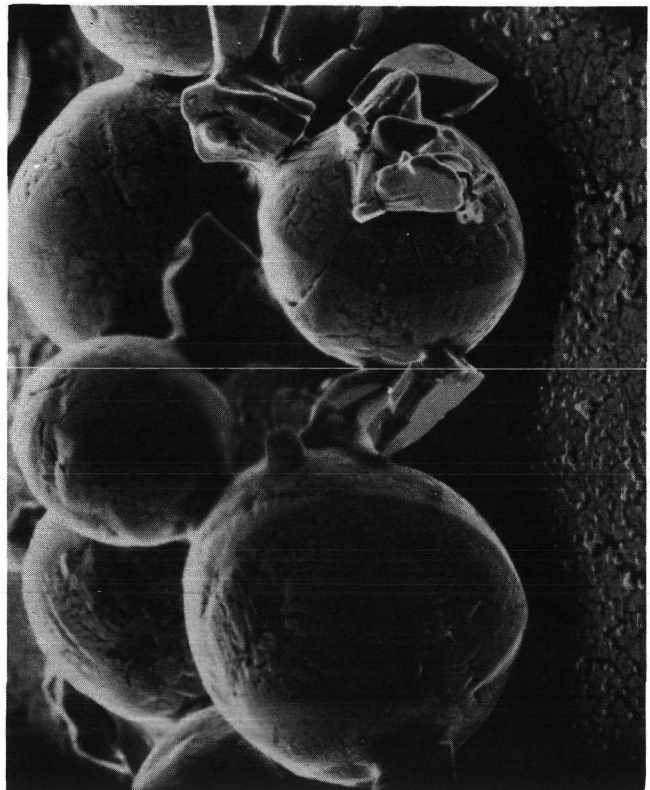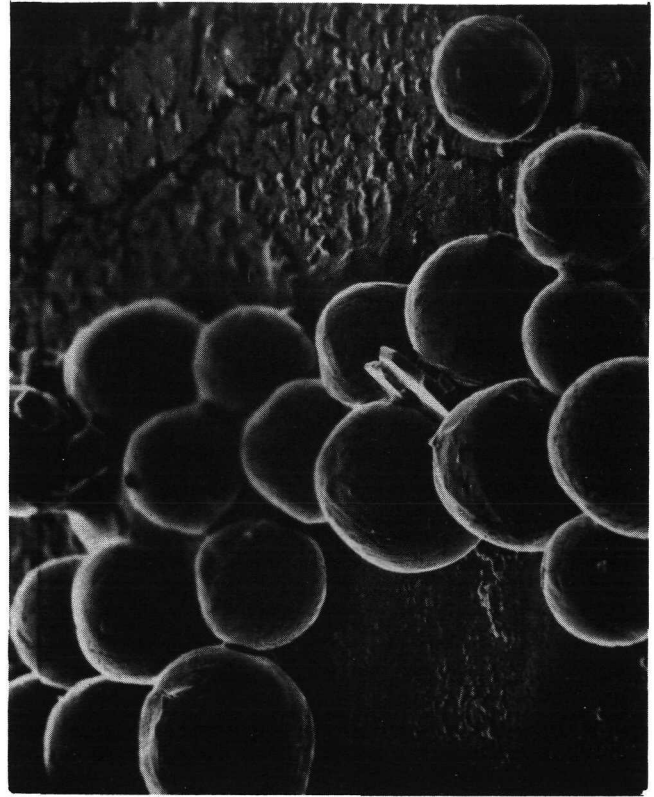FIGURE 10   EXPERIMENTAL SPECTRA OF CORUNDUM BEADS

215X   130μ

500X   35μ

1080X   130μ

1000X   35μ

FIGURE 11 SCANNING ELECTRON MICROGRAPHS OF CORUNDUM BEADS

III-24

sized sample but the particles have been largely de-edged. The changed level of the spectra in the 575 - 900 cm^{-1} region and the noticeably smaller particle size effect when contrasted with the data for comparable sized particles in Figure 5 both confirm the assumed mechanism of edge absorption. We believe that the residual edges in the 35μ beads are largely responsible for the fact that the spectrum of this sample is still somewhat below the spectrum of the 130μ beads in the 575 - 900 cm^{-1} region. We note that the level of the spectrum of the 35μ beads lies between the level of the 60μ and 120μ corundum powders. A dendritic growth can be seen in the scanning electron micrographs of the bead surfaces. This material is apparently responsible for the shape variation in the 630 - 900 cm^{-1} region. Such a result is in accord with a number of theoretical experiments we have conducted by varying the shapes of the asperities (I).

The empirical bridging formula used in the region between 0.3μ and 12μ where both theories are being extended beyond their range of applicability appears to provide better results than either theory alone. This can be seen in Figure 12 where the results of both individual theories and the bridged theory are compared with experimental results for 3.5μ corundum powder. The relatively greater strength of the feature near 535 cm^{-1} with smaller particle size can be seen in the experimental data for the 3.5μ and 10μ particles (Figure 5). This is apparently a residue of the strong fine-particle feature shown by the theory Figure 12) to peak near 570 cm^{-1} and it was used in an attempt to
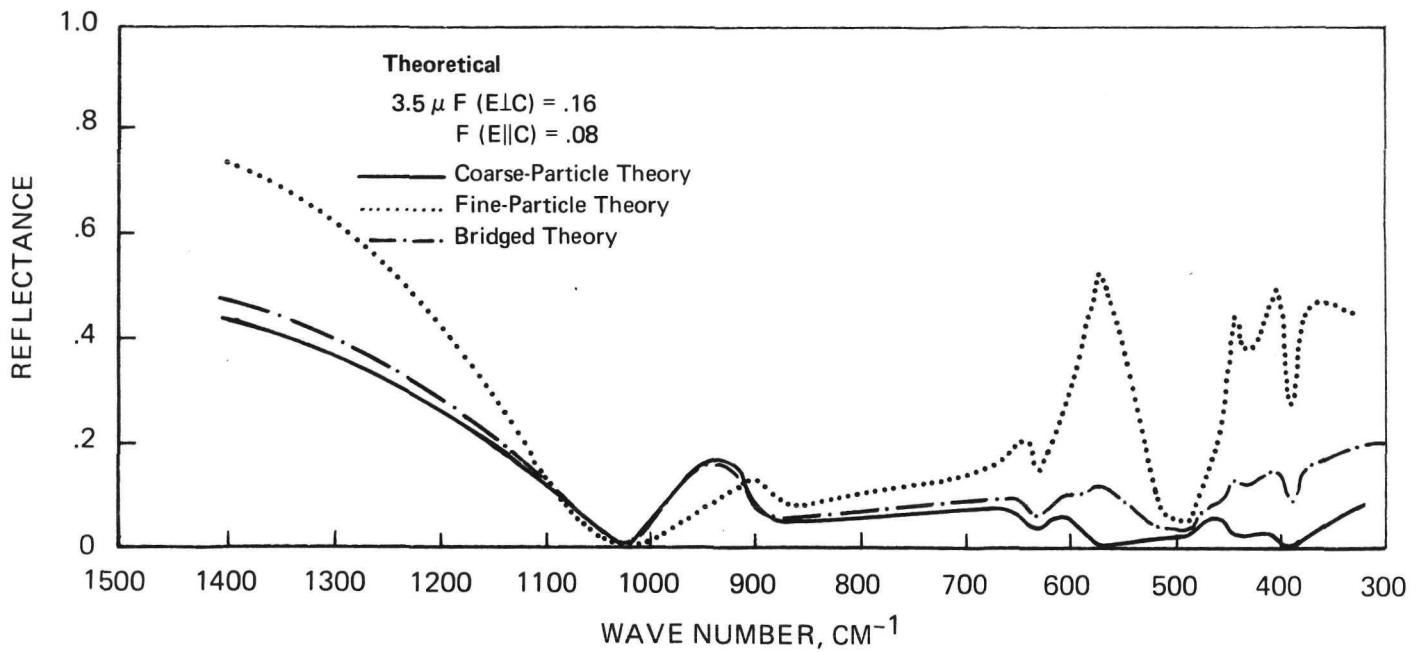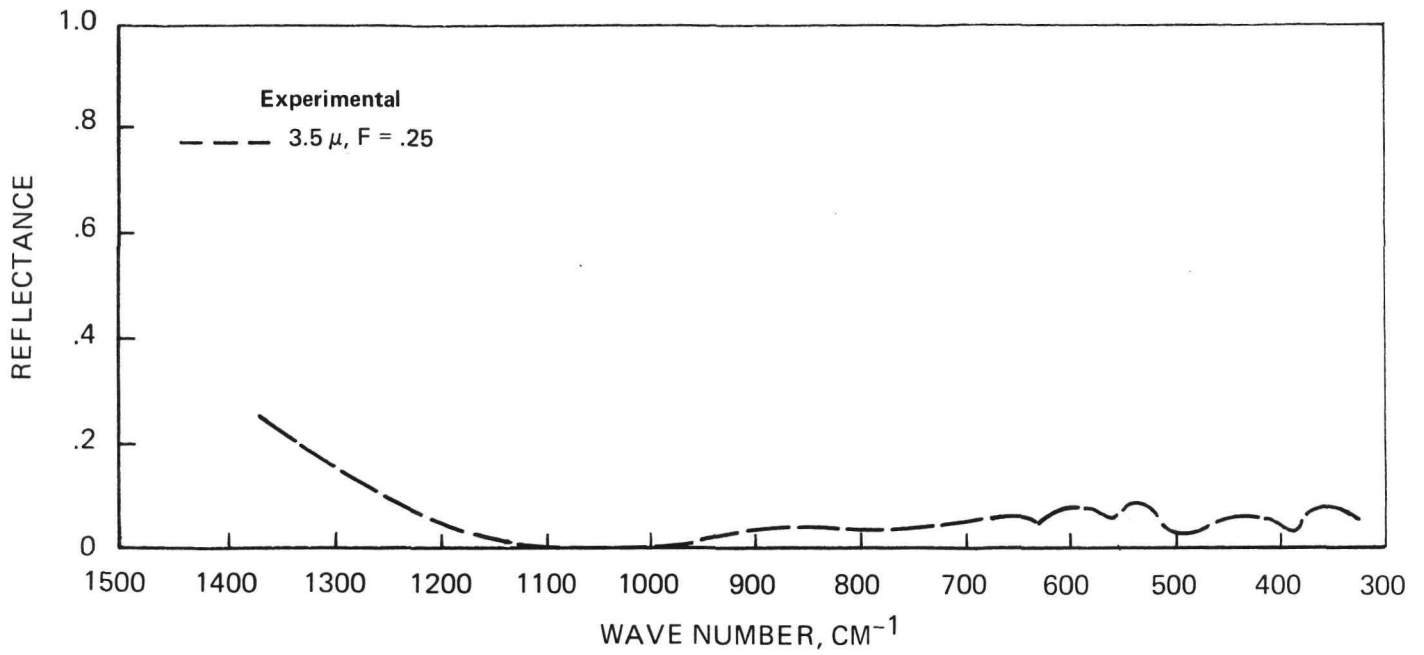
FIGURE 12   COMPARISON OF THE BRIDGED THEORY WITH THE COARSE-PARTICLE
AND FINE-PARTICLE THEORIES FOR CORUNDUM

III–26

Arthur D Little, Inc.

ascertain a reasonable bridging relationship. This relationship
can probably be improved upon, but its optimization is somewhat
dependent on the optimization of the other adjustable factors
as well as the replacement of the monodisperse assumption with a
more realistic particle size distribution function. The real
particles, of course, have a size distribution, but the theoreti-
cal results shown in this paper are all for monodisperse
particles.

Figure 13 shows the theoretical and experimental results for
quartz powders. Once again the theoretical spectra for the
coarser particles do not attain values as high as those observed
in the experimental data in the reststrahlen regions. For the
theoretical runs we assumed no surface asperities, since the
$1100 - 1200 \text{ cm}^{-1}$ feature in quartz, which is similar to the
previously discussed $630 - 900 \text{ cm}^{-1}$ feature in corundum, is
only observed at the smallest particle sizes. However, clinging
fine particles are commonly observed to be present in samples of
larger particle size. In our theory they would act in much the
same way as surface asperities. The data shown for the sample
marked $0 - 20\mu$ provide a good example of the effect of such fines.
The average particle size for this sample is near 10μ but the
effect of the large number (but small volume fraction (0.007) of
particles less than 2.85μ) is such as to give a more pronounced
feature in the $1100 - 1200 \text{ cm}^{-1}$ region than is observed for the
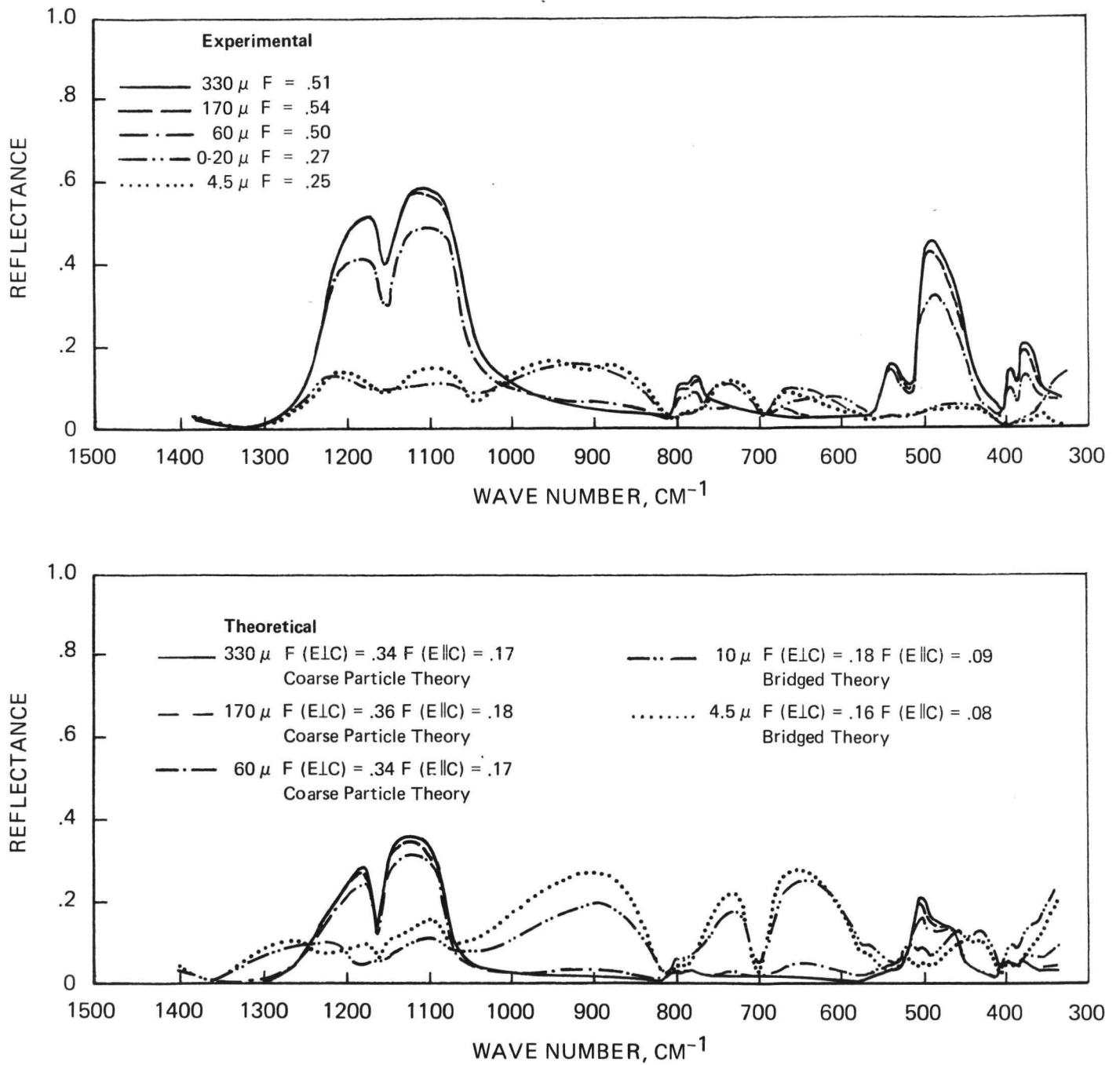4.5μ sample. In fact, the latter sample was obtained only after

FIGURE 13   COMPARISON OF THEORETICAL AND EXPERIMENTAL REFLECTANCE OF QUARTZ POWDERS

III-28

a discrepancy was observed between the experimental particle size and that necessary to produce the feature, using the same value of b, the scale factor for the 1/d edge effect as was used for corundum. That discrepancy led us to reexamine the particle distribution in the 0 - 20μ sample and the wide distribution found suggested that a narrower size range for this important experiment was in order. The 4.5μ sample was then obtained from Duke Standards of Palo Alto, California. They indicate a 1 - 4.5μ range for the sample. Our particle counts give 4.6μ for the volume averaged size of this material, and it has an obviously narrower particle size distribution than the 0 to 20μ sample. The 0 - 20μ sample can be reasonably well fitted by the theory, if we use an asperity factor of NV = 1.5 x 10^{-5} cm to represent the clinging fine particles. This fit tends to confirm our idea that a small volume of clinging fines represents the same kind of extra absorption as do surface asperities. This effect was first observed in some of our early work, when some large quartz particle samples were run as received and after a wet-sieving procedure was used to remove the small volume fraction, but large numbers of clinging fine particles. Figure 14 shows photomicrographs of the samples of quartz powders of large particle size (170μ) as received and after removal of the fines. Figure 15 shows the resultant spectra. The very large effect shown in Figure 15 was produced by a quite small volume fraction of the fines. As with the surface asperities, the effect appears most

Arthur D Little, Inc.

As Received

After Removal of Fines

FIGURE 14 SCANNING ELECTRON MICROGRAPHS (95X) OF 170μ QUARTZ PARTICLES
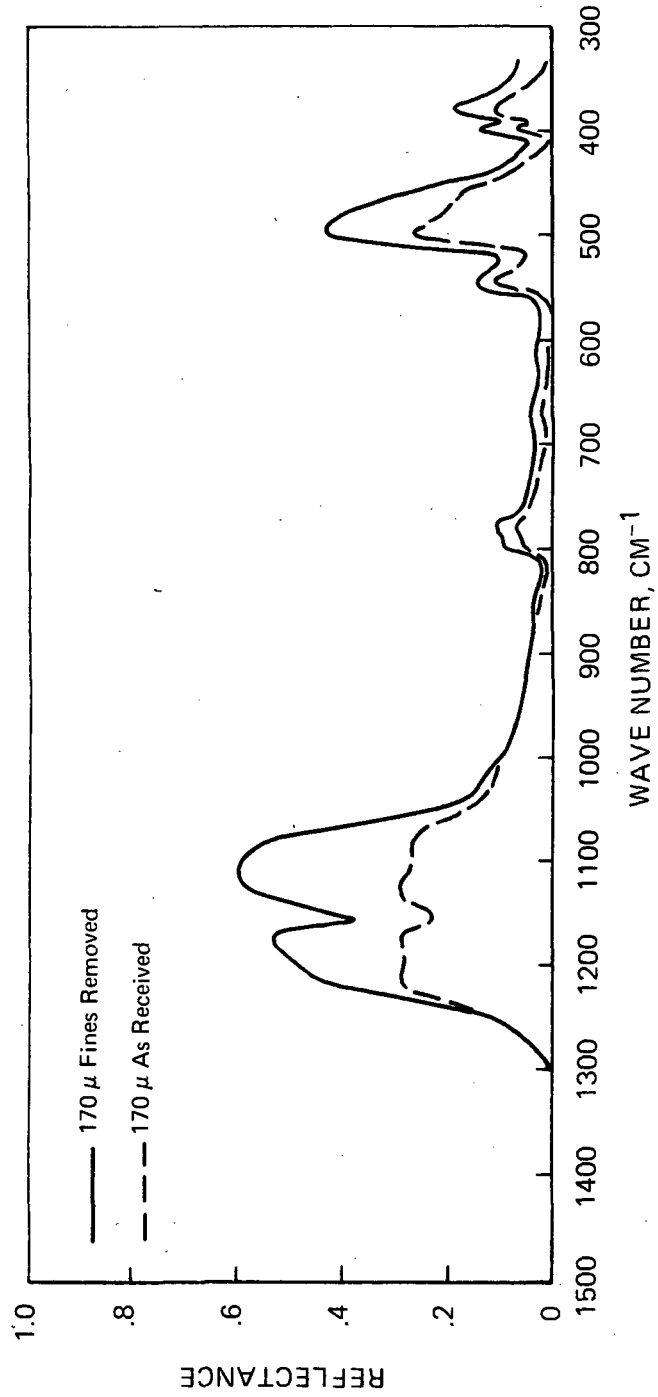
FIGURE 15   EXPERIMENTAL REFLECTANCE OF QUARTZ POWDER:
THE EFFECT OF A SMALL VOLUME OF FINES

III-31

significant in regions of high absorption.

As with corundum we note a theoretical feature (Figure 13) slightly to the high frequency side of the principal reststrahlen band for samples of intermediate particle size (4.5μ and 10μ). This feature does not occur in the experimental data which as before is actually for a particle size distribution. We again note an apparent shift of the reststrahlen feature toward higher frequencies as the particle size is reduced, and believe that the theoretical feature contributes to the shift. It is significant that the feature in question is also produced theoretically in Mie theory calculations[12] for the intermediate particle sizes.

Figure 16 shows experimental and theoretical results for garnet powders obtained from Barton Mines of North Creek, New York. The particle sizes used to calculate the theoretical spectra for these samples were obtained by microscopic techniques. They are slightly larger than the analyses given by Barton Mines. No Surface asperities were invoked in computing the theoretical spectra as microscopic examination showed no need for such a factor. The optical constants used as input parameters for the garnet data were obtained by fitting the spectrum of a large polished sample with a set of classical oscillator parameters, using the Lorentz line shape, by well known techniques[15]. The minor discrepancy observed near 500 cm^{-1} is thought to be due to a slightly deficient set of dispersion parameters, since an insufficient number of points were taken in the spectrum of the single crystal to resolve the small feature by least squares analysis.
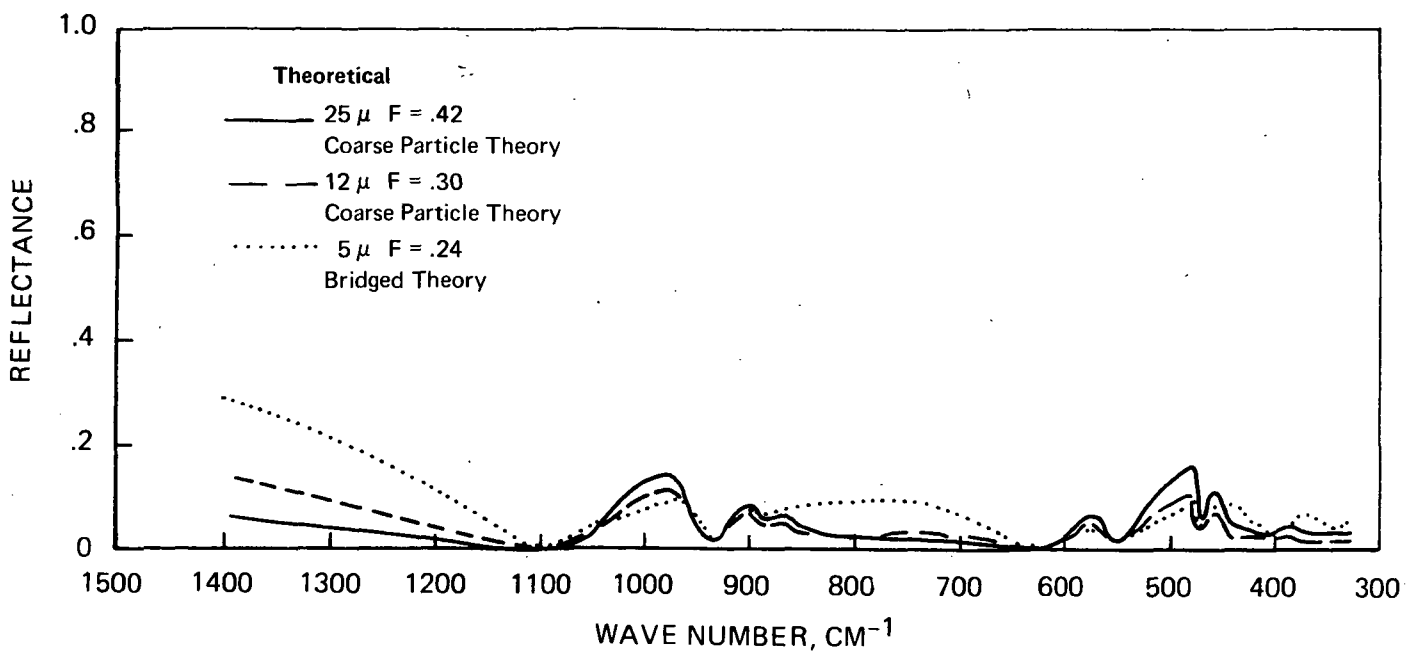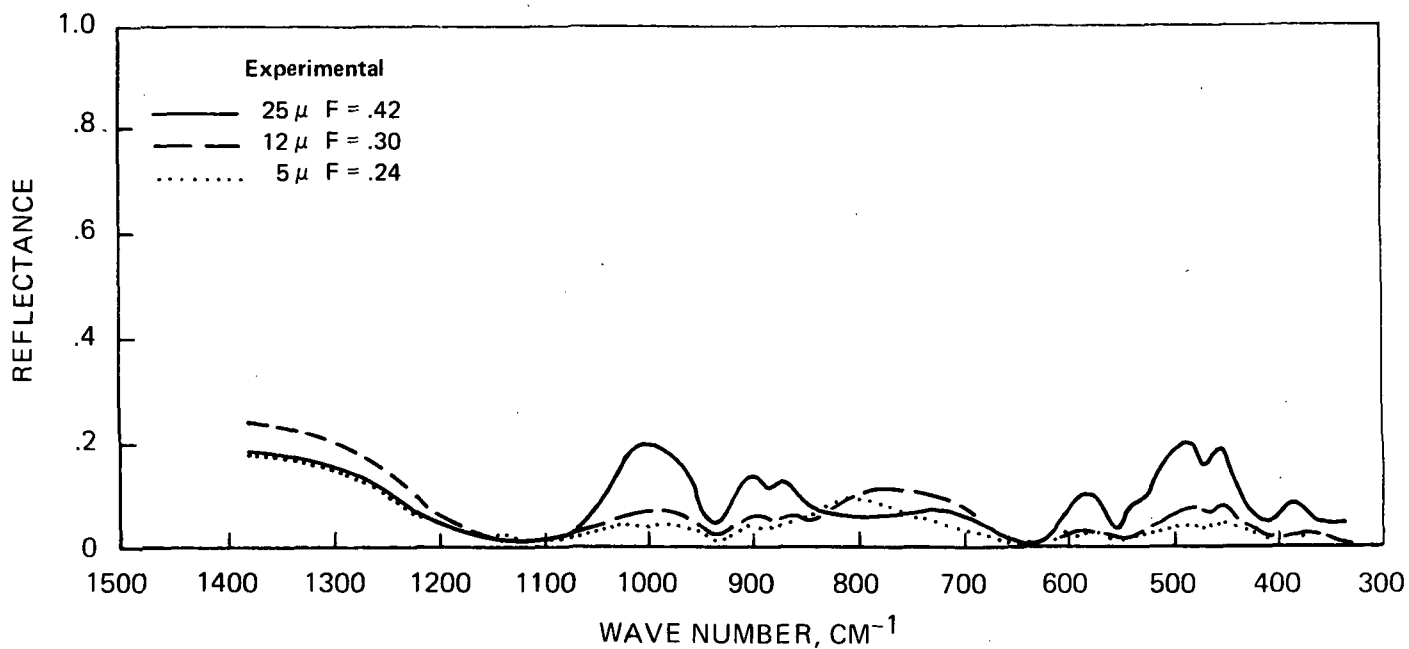
Arthur D Little, Inc.

FIGURE 16   COMPARISON OF THEORETICAL AND EXPERIMENTAL
REFLECTANCE OF GARNET POWDERS

III-33

The experimental and theoretical spectra of two mixtures of quartz and corundum powders are shown in Figure 17. Each mixture actually represents a mixture of four components as quartz and corundum are both uniaxial crystals so that two sets of optical constants are required to represent each of them. In these cases the experimental data were processed using the measured sample temperatures instead of applying the usual Christiansen technique as this technique cannot be justified for the case of mixtures. It is clear from the theoretical results shown in this figure that there is no frequency where the reflectance is zero such as would occur at the principal Christiansen frequency for a pure sample. The experimental results can be seen to confirm this theoretical conclusion. We note that the departure from zero reflectance is substantially greater for the finer particles. Thus arbitrarily setting the lowest point in the spectrum of a mixture at zero reflectance or unit emittance would make a substantially greater error for the finer particle data than for the coarser particle data. It is also quite significant that for the finer particle sample the lowest point in the spectrum occurs near 1160 cm^{-1}. This corresponds to the Christiansen frequency of neither component. Thus an identification technique based on the principal Christiansen frequency would fail for this mixture.
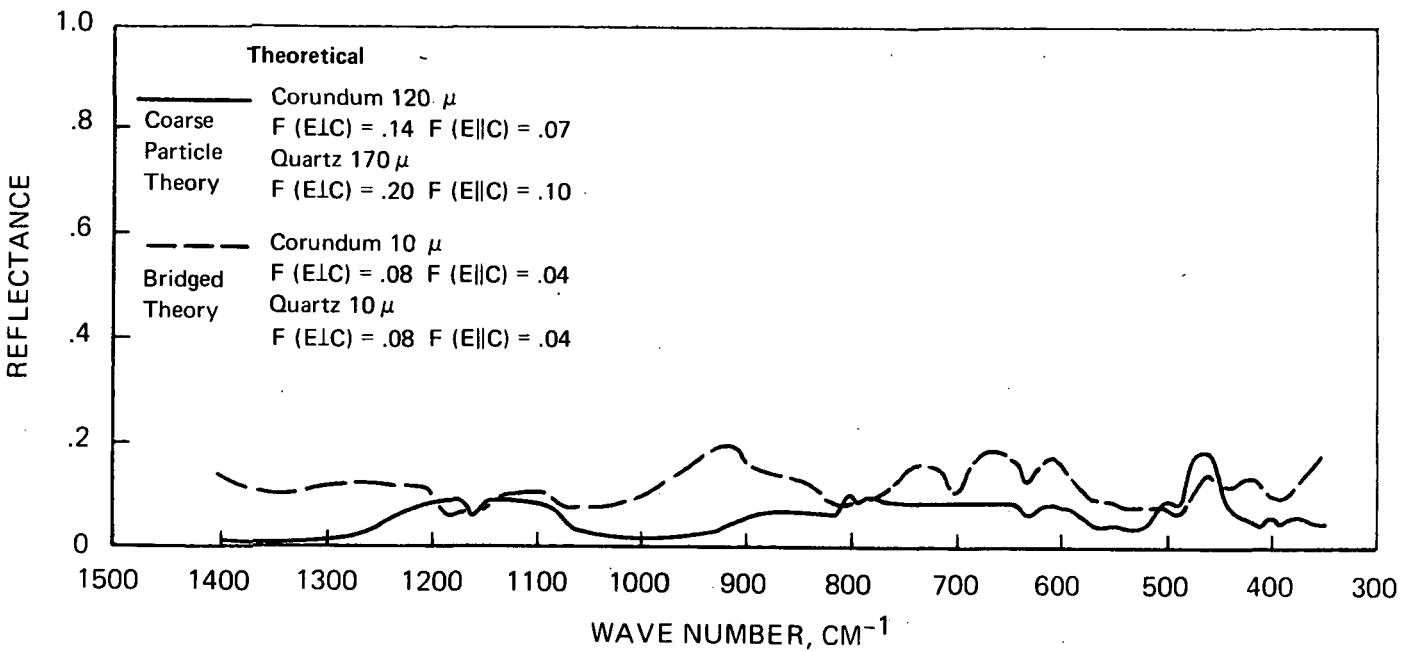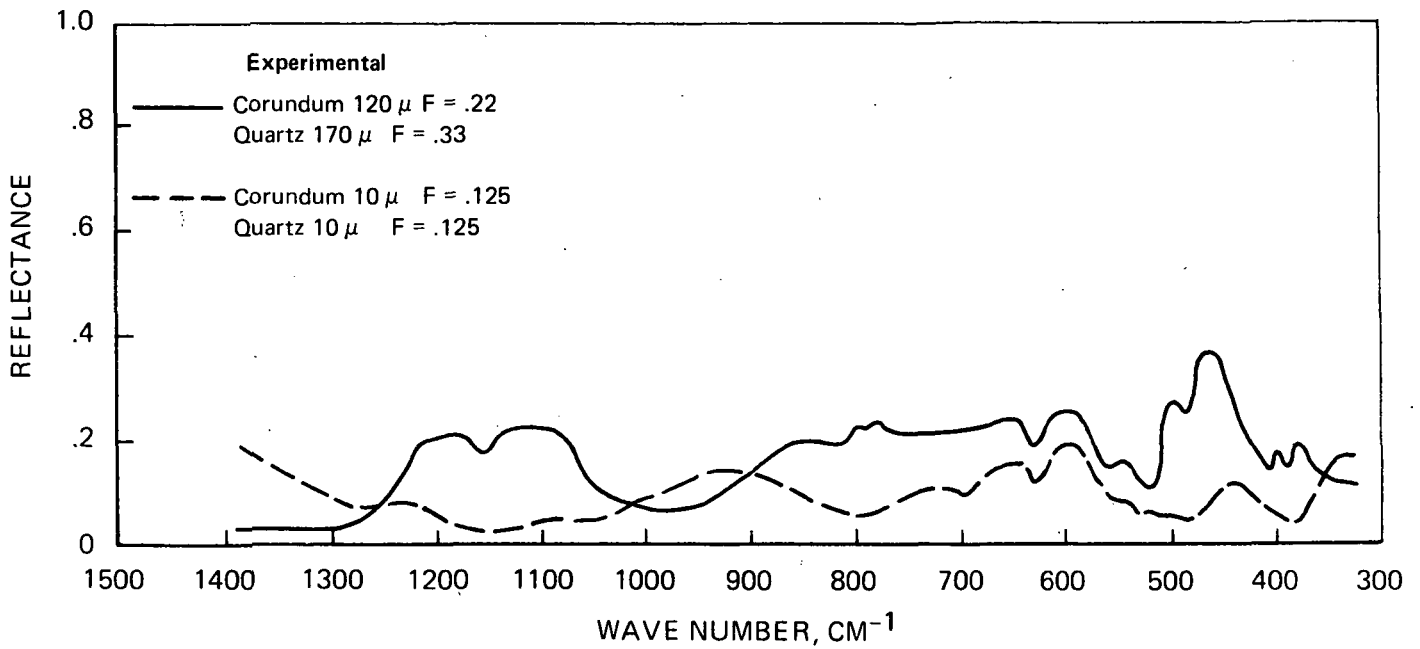
Arthur D. Little, Inc.

FIGURE 17   COMPARISON OF THE THEORETICAL AND EXPERIMENTAL
REFLECTANCE OF MIXTURES OF QUARTZ AND CORUNDUM

Arthur D. Little, Inc.

For both mixtures the shapes of the theoretical spectra quite adequately represent the experimental data. While the general level of the theoretical spectrum of the mixture of finer size powders is also in good agreement with the experimental spectrum, the same cannot be said for the spectrum of the mixture of coarse powders. Once again we believe this discrepancy is due to our use of a continuum model rather than a discrete layer model.

It is worth noting, however, that for remote sensing applications where the problem is the inverse one of determining mineral compositions from spectral data, the general spectral level is much less important than the detailed structure of the spectral features.

ACKNOWLEDGMENT

Arthur D Little, Inc.

REFERENCES

1. W. W. Coblentz, "Investigations of Infra-Red Spectra",
    Carnegie Institution of Washington, 1905, reprinted by the
    Coblentz Society, 1962.

2. R. A. Hanel, B. J. Conrath, W. A Hovis, V. G. Kunde,
    P. D. Lowman, J. C. Pearl, C. Prabhakara, B. Schlachman
    and G. Levin, Science, 175, 305 (1972).

3. R. A. Hanel, B. J. Conrath, V. G. Kunde, C. Prabhakara,
    I. Revah, V. V. Salomonson and G. Wolford, J. Geophys.
    Res. 77, 2629, (1972).

4. J. R. Aronson, A. G. Emslie and H. G. McLinden, Science
    152, 345, (1966).

5. R. J. P. Lyon, NASA CR100, Washington, D. C., 1965.

6. W. A. Hovis, Jr., and W. R. Callahan, J. Opt. Soc. Am.,
    56, 639, (1966).

7. G. R. Hunt and R. K. Vincent, J. Geophys Res., 73, 6039, (1968).

8. A. G. Emslie in Progress in Astronautics and Aeronautics,
    (Academic Press, Inc., New York, 1966) Vol 18.

9. A. G. Emslie and J. R. Aronson, Appl. Opt. preceding paper, 1973.

10. J. R. Aronson and A. G. Emslie, The Moon, 5, 3 (1972).

11. J. R. Aronson, A. G. Emslie, T. P. Rooney, I. Coleman and
    G. Horlick, Appl. Opt., 8, 1639, (1969).

12. J. E. Conel, J. Geophys. Res., 74, 1614, (1969).

13. A. S. Barker, Jr., Phys. Rev., 132, 1474, (1963).

14. W. G. Spitzer and D. A. Kleinman, Phys. Rev., 121, 1324, (1961).

15. H. W. Verleur, J. Opt. Soc. Am., 58, 1356, (1968).

IV. MODIFICATIONS IN THE THEORY

DISCRETE-LAYER MODEL

In Section II, pp 46-48, we outlined a discrete-layer model that describes the radiative transfer in media composed of closely-packed coarse particles much more realistically than can be done by a continuum model in which scattering and absorption are regarded as continuously distributed parameters. Since writing the paper we have extended the discrete-layer model to include the effect of diffuse scattering by asperities on the surfaces of the particles.

We consider a parallel beam of radiation of intensity I_o incident at an angle θ on an element of area dA of the surface of a particle. Then the reflected power is

$$P = R_o I_o \, dA \cos\theta \qquad (1)$$

where R_o is the diffuse reflectance.

For simplicity we assume that the reflected radiation is Lambertian, so that the angular distribution has the form

$$dP = \frac{P}{\pi} \cos\chi \, d\omega \qquad (2)$$

where χ is measured from the normal to dA and $d\omega$ is an element of solid angle.

Arthur D. Little, Inc.

We now resolve the diffuse radiation into discrete beams along the normal and tangential directions by means of our $\cos^2\chi$, $\sin^2\chi$ weighting factors. We find that the radiation splits equally between these directions:

$$P_{normal} = \frac{1}{2} R_o I_o \cos\theta \, dA \tag{3}$$

$$P_{tangential} = \frac{1}{2} R_o I_o \cos\theta \, dA \tag{4}$$

Here Eq. (4) represents the sum of four discrete tangential beams.

We next resolve these beams by the same method into back, transverse, and forward components relative to the original incident beam. The results, expressed as differential scattering crosssections, are

$$d\sigma_{back} = \frac{1}{2} R_o dA \left(\frac{1}{4} \cos\theta \sin^2\theta + \cos^3\theta\right) \tag{5}$$

$$d\sigma_{transverse} = \frac{1}{2} R_o dA \left(\frac{1}{2} \cos\theta + \frac{1}{2} \cos^3\theta + \cos\theta \sin^2\theta\right) \tag{6}$$

$$d\sigma_{forward} = \frac{1}{2} R_o dA \left(\frac{1}{4} \cos\theta \sin^2\theta\right) \tag{7}$$

The sum of these crosssections is $R_o dA \cos\theta$, as it should be.

To obtain the total particle crosssections for transverse and backward external reflection we replace dA by $2\pi a^2 \sin\theta \, d\theta$ in (6) and (5) and integrate with respect to θ:

$$\sigma_{refl,t} = \pi a^2 \int_0^{\pi/2} R_o \left(\frac{1}{4} + \frac{1}{4}\cos^2\theta + \frac{1}{2}\sin^2\theta\right) \sin2\theta d\theta \tag{8}$$

$$\sigma_{refl,b} = \pi a^2 \int_0^{\pi/2} R_o \left(\frac{1}{8}\sin^2\theta + \frac{1}{2}\cos^2\theta\right) \sin2\theta d\theta \tag{9}$$

IV-2

These formulas replace the specular reflection formulas (12) and (13) in Section II. The diffuse-reflection values of $\sigma_{refl,b}$ and $\sigma_{refl,t}$ are used in (74) and (75) of Section II in the calculation of σ_t and σ_b, which in turn enter into the evaluation of the reflectance and absorptance ρ and α of a monolayer of particles through (86) and (87) of Section II. Eq. (88) then gives the reflectance of the powder.

In the case of a mixture of particles of approximately equal size we calculate the quantities ρ_j and α_j from (86) and (87) for each kind of particle separately as though it were present alone at the volume fraction f. Then we determine the average values $\bar{\rho}$ and $\bar{\alpha}$ by the formulas

$$\bar{\rho} = \Sigma f_j \rho_j \tag{10}$$

$$\bar{\alpha} = \Sigma f_j \alpha_j \tag{11}$$

where f_j is the volume fraction of mineral j, excluding vacuum.

We have not yet generalized the discrete-layer model to the case of particles with a wide distribution of sizes.

CONTACT FACTOR

In our report of April 1, 1971, pp 9-12 we derived an expression for the effective fraction G of the surface area of a particle available for scattering after allowance is made for the effect of optical bonding near the points of contact with neighboring particles.

Arthur D Little, Inc.

The "contact factor" G was given by

$$G = 1 - \frac{0.6 \, f \, \lambda_o}{d} \tag{12}$$

where f, λ_o, and d are the volume fraction of particles, the free-space wavelength, and the particle diameter, respectively.

In using this formula to correct the scattering coefficient S we encountered two difficulties. The first is that G drops abruptly to zero when d falls below a certain critical value. The second is that (12) does not allow for the fact that the concept of optical bonding breaks down in spectral regions where the particles are opaque.

We can avoid both difficulties by modifying (12) to read

$$G = e^{-0.6 \, f \, \lambda_o \, T/d} \tag{13}$$

where

$$T = e^{-4\pi k d/\lambda} \tag{14}$$

is the transmission factor along a particle diameter. One sees that in spectral regions where the particles are opaque, T = 0 and G = 1. Therefore the contact factor has no effect. As the particle diameter decreases the exponent of (13) increases and G tends to zero continuously.

We include the factor G in the theory as a multiplicative factor which modifies the scattering crosssections σ_t and σ_b. The effect is to reduce the scattering, and therefore the reflectance, for transmitting particles only.

IV-4

COMPARISON WITH EXPERIMENT

Figures 1, 2 and 3 show the results of using the discrete-layer model and the new contact factor to fit the experimental data of Figures 5, 13, and 17 of Section III. A considerable improvement can be seen in the reflectance level in the reststrahlen bands for the coarser particles. Some increase in the level resulting from the discrete-layer model for those regions where the particles are semi-transparent was effectively nullified by the contact factor.

The use of the coarse particle theory instead of the bridged theory for the 10μ particles would have resulted in a slightly lower spectral level but only at the expense of introducing some minor shape discrepancies. No attempt was made to reoptimize the bridging formula. The comparison between these three figures and their analogs in Section III demonstrates the essential validity of the discussion of Section II concerning the failings of a continuum model.

Arthur D. Little, Inc.

Experimental

— 120 μ, F = .48
— — 60 μ, F = .49
- - - - 30 μ, F = .39
—·—· 10 μ, F = .30
—··— 3.5 μ, F = .25
········ 0.3 μ, F = .19 (Compressed)

REFLECTANCE

WAVE NUMBER, CM^{-1}

Theoretical

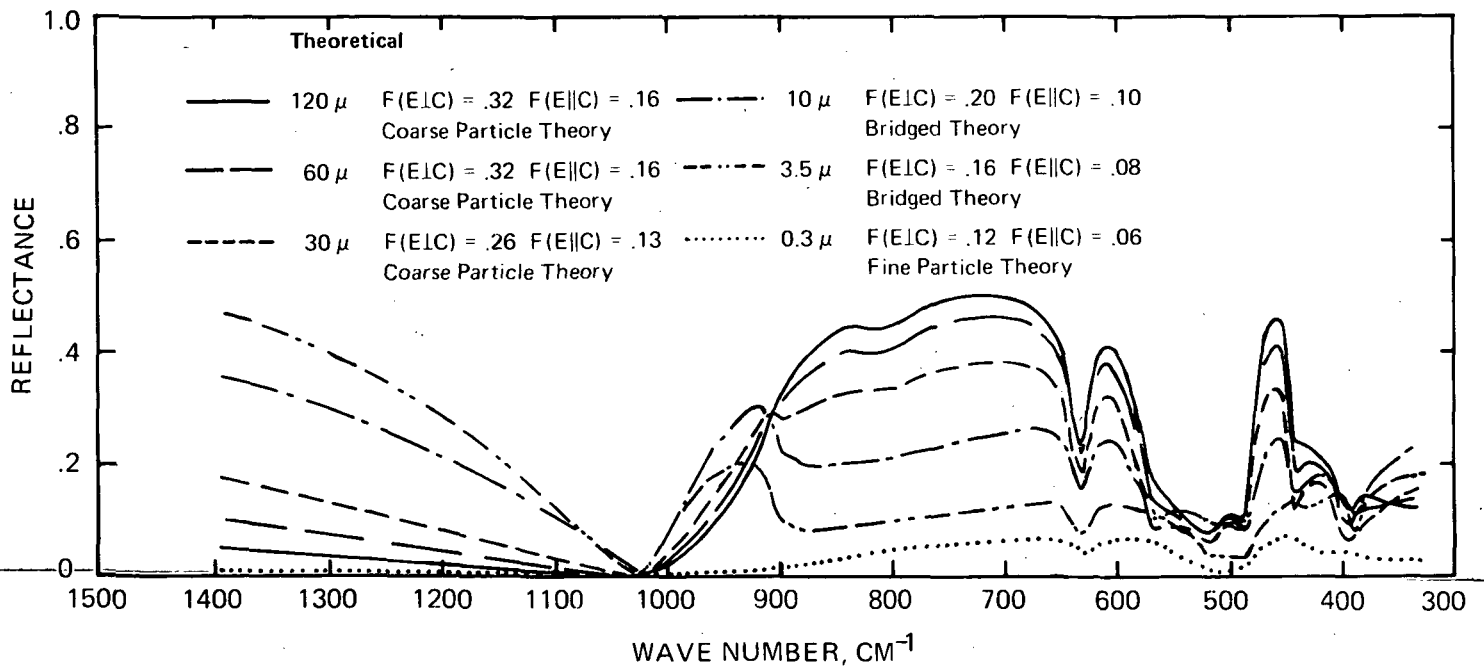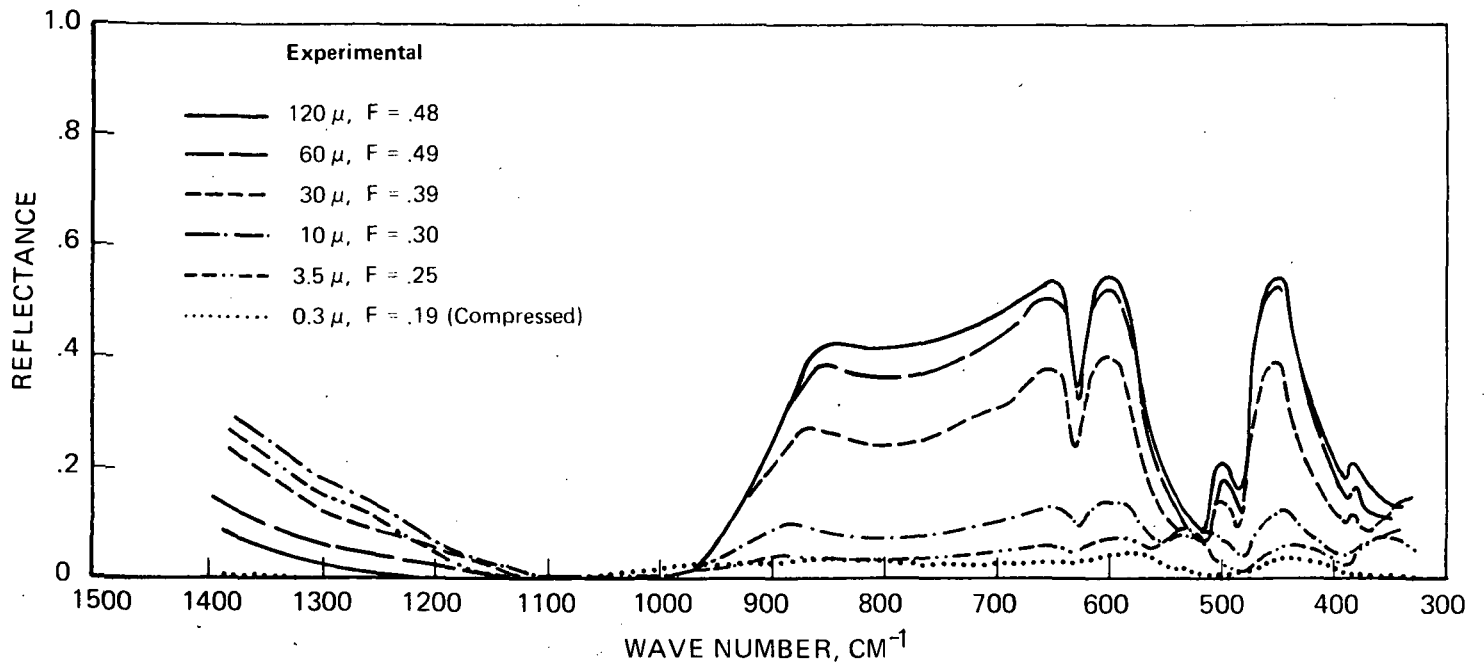|			
— 120 μ	F(E⊥C) = .32 F(E∥C) = .16 Coarse Particle Theory	—·— 10 μ	F(E⊥C) = .20 F(E∥C) = .10 Bridged Theory
— — 60 μ	F(E⊥C) = .32 F(E∥C) = .16 Coarse Particle Theory	—··— 3.5 μ	F(E⊥C) = .16 F(E∥C) = .08 Bridged Theory
- - - 30 μ	F(E⊥C) = .26 F(E∥C) = .13 Coarse Particle Theory	········ 0.3 μ	F(E⊥C) = .12 F(E∥C) = .06 Fine Particle Theory

REFLECTANCE

WAVE NUMBER, CM^{-1}

FIGURE 1   COMPARISON OF THEORETICAL AND EXPERIMENTAL REFLECTANCE OF CORUNDUM POWDERS
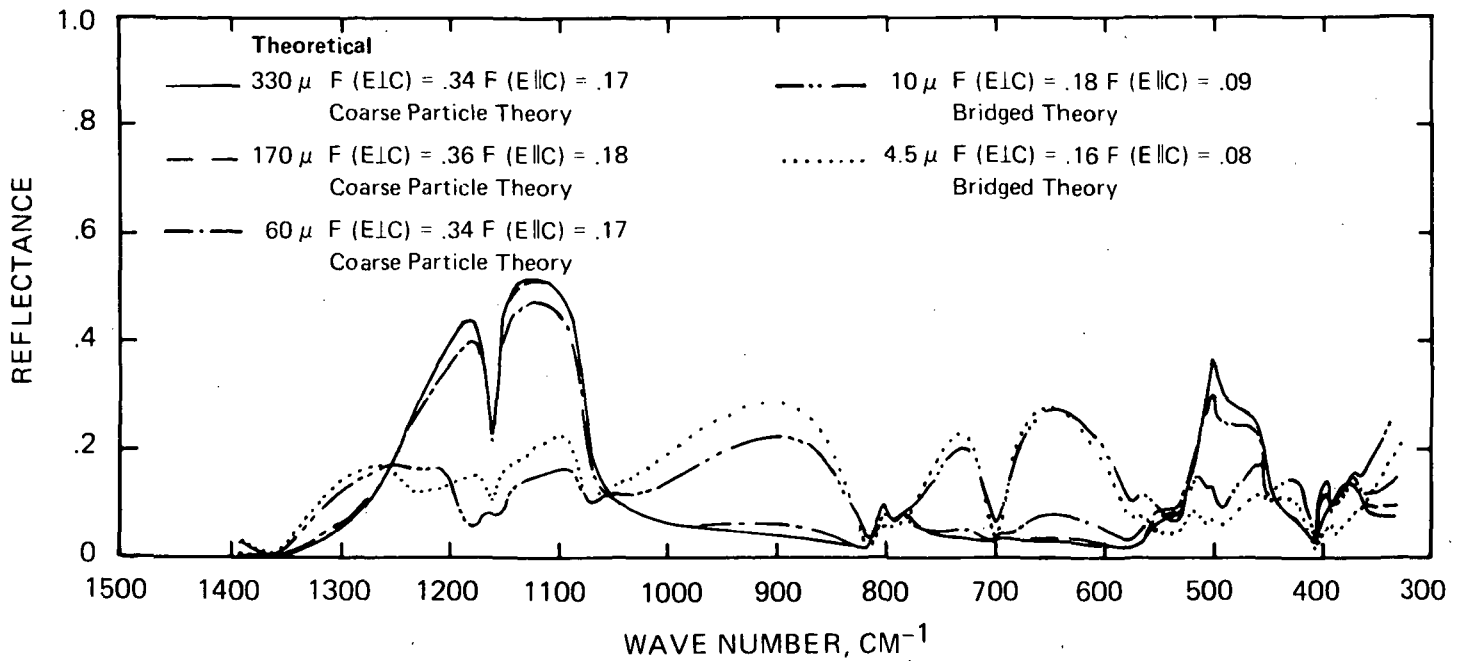
Arthur D. Little, Inc.
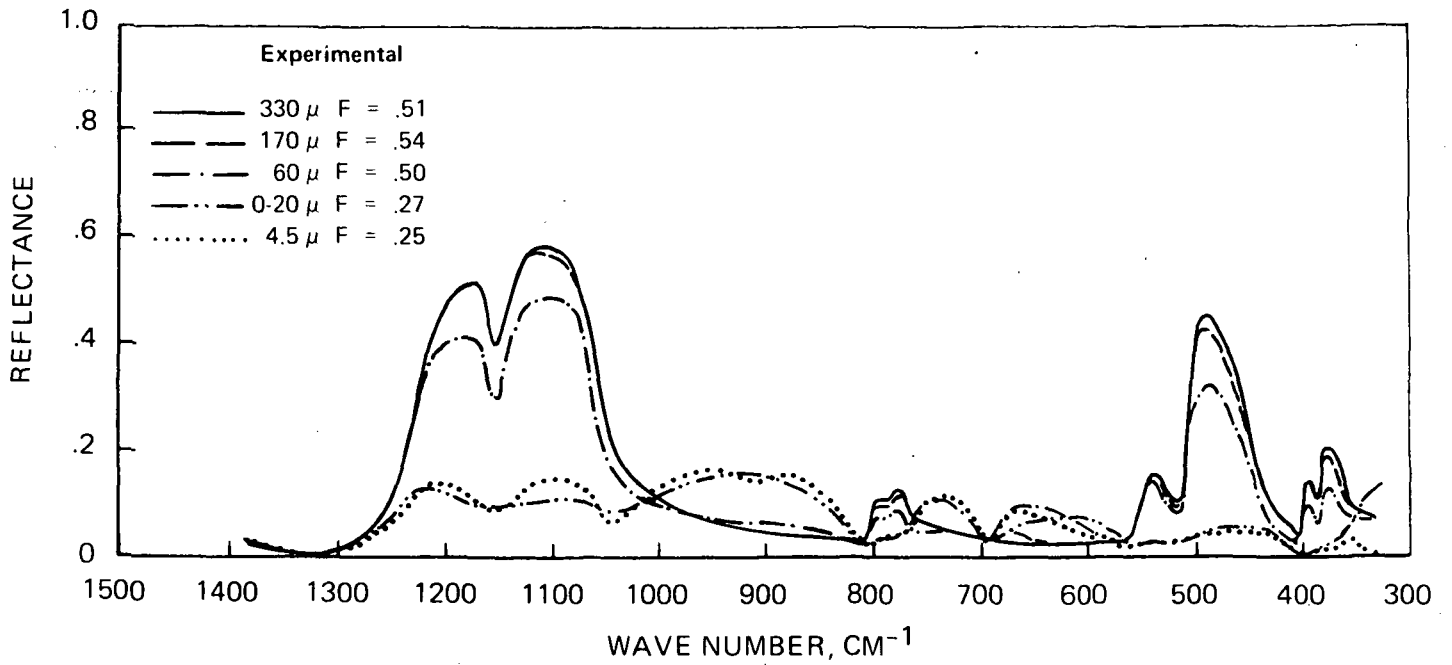
FIGURE 2   COMPARISON OF THEORETICAL AND EXPERIMENTAL REFLECTANCE OF QUARTZ POWDERS
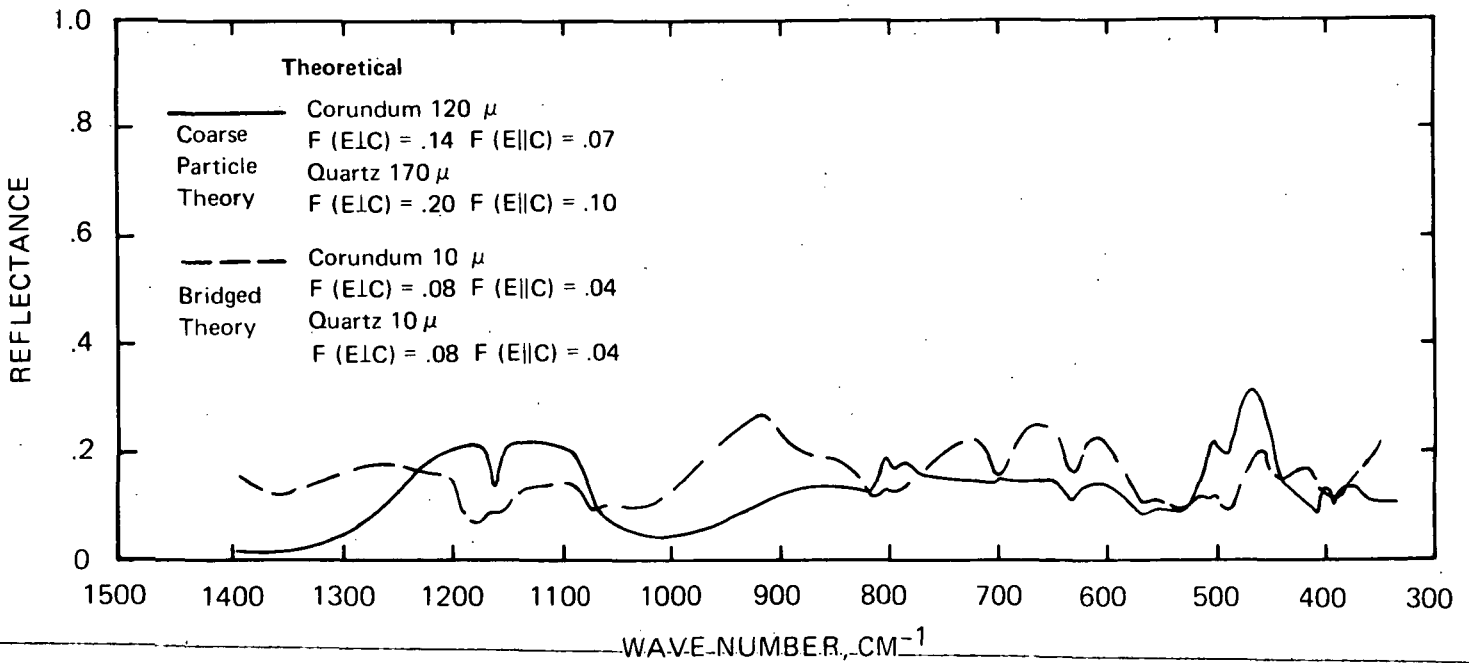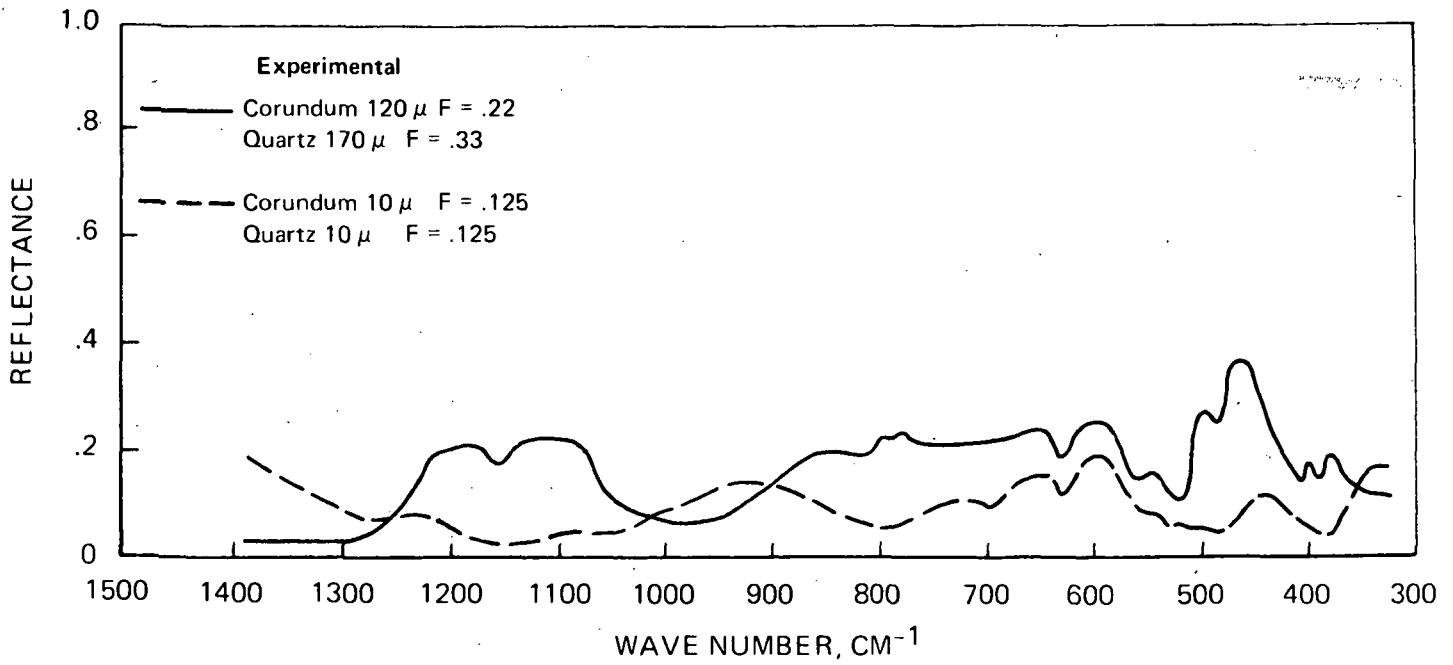
Arthur D Little, Inc

FIGURE 3   COMPARISON OF THE THEORETICAL AND EXPERIMENTAL REFLECTANCE OF MIXTURES OF QUARTZ AND CORUNDUM

IV-8

V. THE INVERSE PROBLEM

The inverse problem consists finding a suitable way to use the
theory of reflectance to analyze the experimental spectrum of an
unknown mixture of powdered minerals in order to derive quantitative
information about volume fractions (f_j) and particle sizes (d_j)
of the minerals (j). It is assumed, of course, that the mixture
contains a reasonably small number of candidate minerals of known
optical constants.

Our theory indicates quite strongly that a simple linear mixing
rule for reflectances is not a good basis for the inverse problem.
For example, Figure 1 shows the variation of reflectance predicted by
the continuum model, described in Sections II and III, as a function
of the relative proportions of the two components in quartz-corundum
mixtures. The five frequencies chosen illustrate examples of rather
different behavior. The important point is the significant non-linearity
of the curves, the extreme example being that for 630 cm^{-1}.

A further consideration is that no theory could possibly include
all of the parameters needed to describe a real mixture, such as the
particle size distributions of all component minerals, the nature of the
surface asperities on each type of particle, the degree of aggregation,
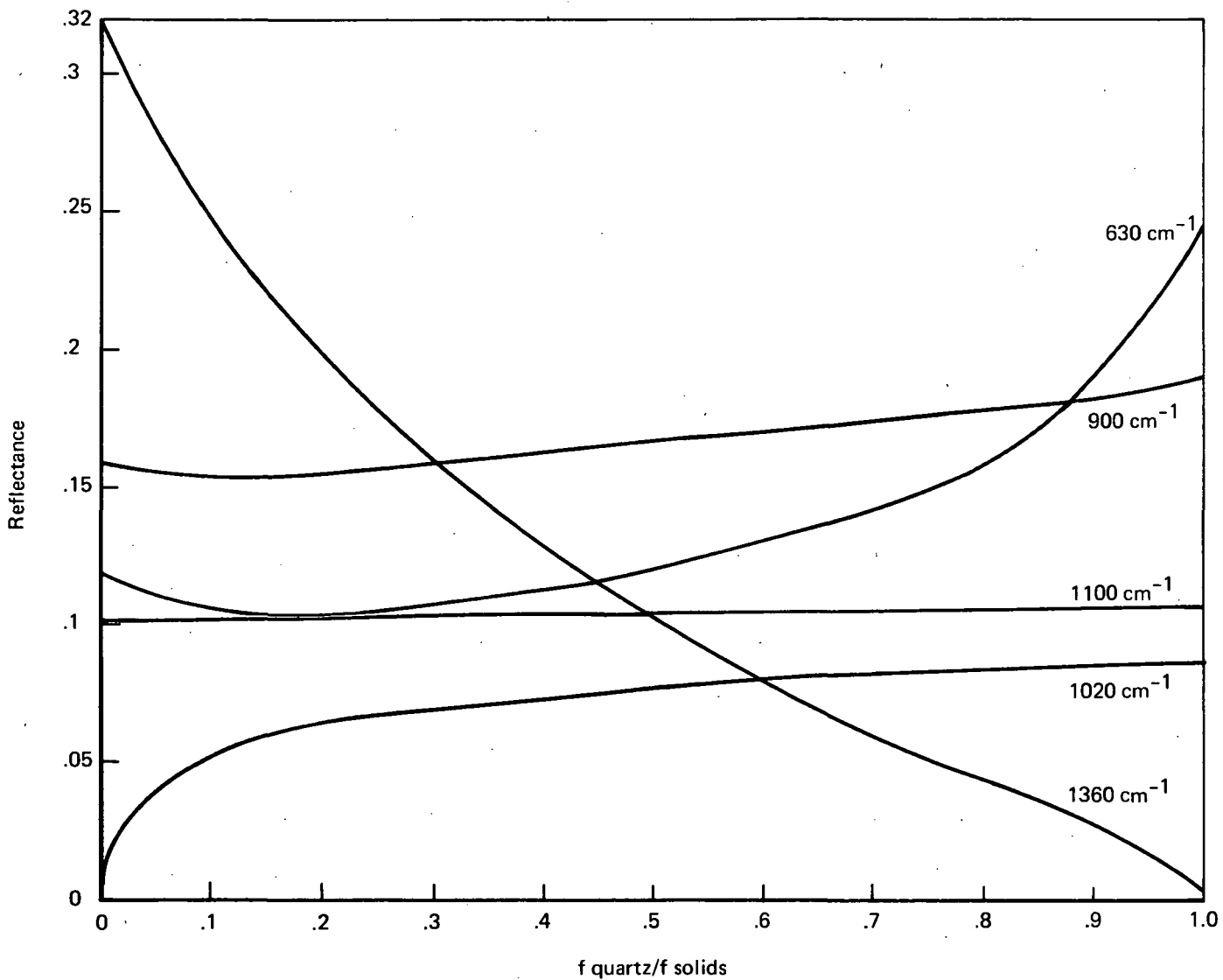etc. This means that the theoretical spectrum will always differ

FIGURE 1   THEORETICAL VARIATIONS IN REFLECTANCE WITH THE MIXING RATIO IN MIXTURES
OF CORUNDUM AND QUARTZ (10μ powders)

quantitatively from the experimental spectrum even with the optimum

choice of the adjustable theoretical parameters. Such differences will

occur in spectral level and in the detailed shape of the spectral bands.

It appears, however, that the locations of the maxima and minima of the

experimental and theoretical spectra agree quite well, for optimum

values of the theoretical parameters, and that the ordering of the

peaks and valleys with respect to amplitude is about the same for both

spectra.

On the basis of these considerations we have developed a new

quantitative method for comparing a theoretical spectrum with an

experimental one. The method pays attention only to the ordering of the

amplitudes in each spectrum at a number of frequencies selected from

the experimental spectrum on the basis of features of interest such

as peaks, valleys, abrupt changes of slope, etc. Some twenty to thirty

frequencies are often sufficient to characterize an infrared spectrum.

After selection of N frequencies we compare the amplitude at

the first frequency with the amplitudes at the other N-1 frequencies,

and record a +, 0, or - at each of these frequencies depending on

whether the amplitude is greater than, equal to, or less than that at

the first frequency. We then repeat the comparison starting with the

second frequency and comparing its amplitude with those of the succeeding

N-2 frequencies. On continuing the process we obtain a triangular

matrix of N(N-1)/2 elements which have the symbols +, 0, or -. This

Arthur D. Little, Inc.

matrix characterizes the characteristic shape of the experimental

spectrum. The symbol 0 is assigned when the amplitudes at two fre-

quencies are equal within some noise level.

We now compute a theoretical spectrum, for a set of assumed values

of the f_j and the d_j, and characterize it in the same way as for

experimental spectrum, using the same set of N selected frequencies.

Next we compare the theoretical and experimental matrices and

count the number of coincidences in the two sets of N(N-1)/2 elements.

The final score, which lies between 0 and N(N-1)/2, is a quantitative

measure of the degree of fit between the theoretical and experimental

spectra and can be used as the criterion for determining the optimum

theoretical parameters.

A computer program was constructed to carry out such an analysis

of our data. It was used for two mixtures of quartz and corundum. The

coarse-particle theory results were used for the 170μ quartz-120μ

corundum mixture, and the bridged theory for the 10μ mixture. The

procedure used the continuum model theory and so its facility for

ignoring the spectral level was more severely tested than would presently

be the case. The analysis was carried out in each example after choosing

20 spectral points from the experimental data. Figure 2 shows the coinci-

dence scores for each of the chosen ratios of the components. The

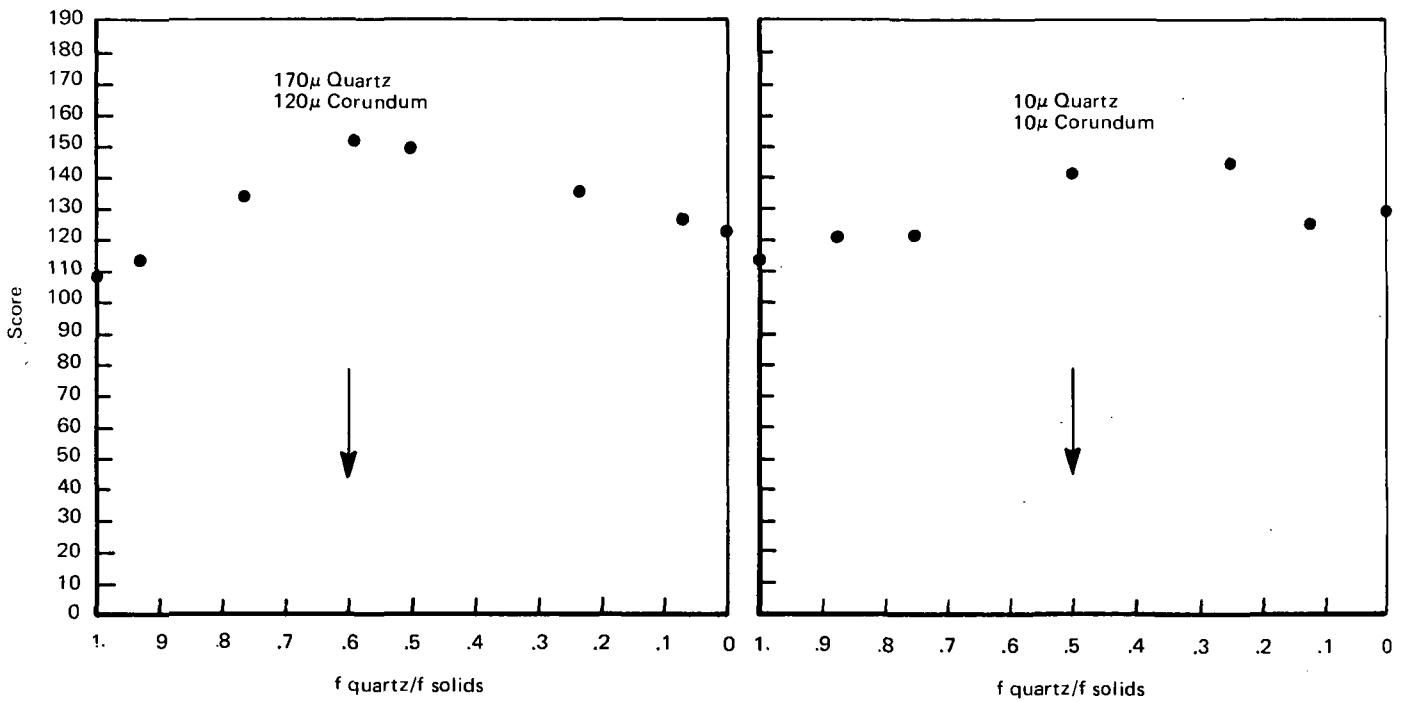arrows indicate the measured ratios in the real mixtures, but it must

FIGURE 2   ESTIMATE OF THE RELATIVE AMOUNTS IN MIXTURES OF CORUNDUM AND QUARTZ

be recognized that this ratio is the average for the entire sample, ...

and may not describe the top layer where the measured radiation originates.

No attempt has yet been made to interpolate between the individual

theoretical results although this could clearly be done. An increase

in the number of spectral points would also almost certainly improve

the technique as 20 points did not sufficiently describe all features

in the spectrum. We consider that this initial success should be

readily extendable to mixtures having more components.

Arthur D Little, Inc.

VI. CONCLUSIONS

The research program described in the current and preceeding[1,2,3] reports has resulted in the development of a comprehensive new theory of the spectral reflectance (or emittance) of particulate materials. The theory has been shown to give excellent agreement with experimental measurements of the infrared emittance spectra of particulate minerals and mixtures of minerals over a wide range of particle sizes and packings.

The theory consists of two subtheories. The coarse particle theory is based mainly on geometrical optics, involving the effects of reflection, refraction and absorption. However, certain wave optical considerations are required as the model consists essentially of an assemblage of randomly contacting large spheres that have a degree of surface roughness. The surface roughness is represented by a distribution of ellipsoidal sub-particles for which the absorption and scattering are calculated by wave optics. The loss of scattering efficiency due to optical bonding at the points of contact is also calculated by wave optics. For fine particles, the theory includes a modification of the Lorentz-Lorenz theory to the case of ellipsoidal particles and the use of Rayleigh scattering by such particles considered to be immersed in the Lorentz-Lorenz medium. The two theories are empirically bridged to cover the intermediate region of particle sizes.

In addition, a new method has been devised to treat the inverse
problem of analysis of the spectrum of an unknown mixture. This method
correlates the characteristic spectral features with those predicted
by the theory and searches for a best fit. At the same time it minimizes
the effects of discrepancies in the absolute levels of the spectra. We
anticipate that this method will prove very useful in the analysis of
the spectra of planetary surfaces.

Arthur D Little, Inc.

References

1. J. R. Aronson and A. G. Emslie, "Development of a Theory of the Spectral Reflectance of Minerals," Report to NASA, Manned Spacecraft Center, October 1969 (Contract NAS 9-8396).

2. J. R. Aronson, A. G. Emslie, L. H. Roach, P. F. Strong, and P. C. von Thuna, "Development of a Theory of the Spectral Reflectance of Minerals, Part II," Report to NASA, Manned Spacecraft Center, April 1971 (Contract NAS 9-10875).

3. J. R. Aronson, A. G. Emslie, L. H. Roach, E. M. Smith and P. C. von Thuna, "Development of a Theory of the Spectral Reflectance of Minerals, Part III," Report to NASA, Manned Spacecraft Center, January 1972 (Contract NAS 9-10875).

VII. SUGGESTIONS FOR FURTHER IMPROVEMENTS

Further work could profitably be undertaken in a number of areas.

A. **Methods of Treating Particle Size Distributions**

This is expecially important with regard to the discrete layer model which at present is valid only for mixtures of particles of comparable diameters.

B. **Extension of the Method of Dealing with The Inverse Problem to More Complicated Mixtures**

C. **Further Study of the Effects of Thermal Gradients**

We have carried out some work in this area[1,2], but a better understanding of the experimental data in this regard is still required.

D. **The Effects of Particle Aggregations**

E. **Methods for Handling Biaxial Crystallites**

F. **Extension of the Theory to Particulate Media Having Near Zero Porosity**

The coarse particle theory presently assumes that any ray passes from one material to the next via the void space. This may not always be true.

G. **Resolution of a Minor Discrepancy**

For intermediate size particles, there is an apparent discrepancy between theory and experiment near 930 cm^{-1} for corundum and near 1280 cm^{-1} for quartz. While we believe that the problem relates to the monodisperse assumption used in the theoretical computations (see Section III) the problem requires further investigation.

Arthur D Little, Inc.

References

1. J. R. Aronson, A. G. Emslie, L. H. Roach, P. F. Strong, and P. C. von Thuna, "Development of a Theory of the Spectral Reflectance of Minerals, Part II," Report to NASA, Manned Spacecraft Center, April 1971 (Contract NAS 9-10875).

2. J. R. Aronson, A. G. Emslie, L. H. Roach, E. M. Smith and P. C. von Thuna, "Development of a Theory of the Spectral Reflectance of Minerals, Part III," Report to NASA, Manned Spacecraft Center, January 1972 (Contract NAS 9-10875).